

# A survey of methods for brain tumor segmentation-based MRI images

Yahya M. A. Mohammed<sup>1,\*</sup>, Said El Garouani<sup>2</sup> and Ismail Jellouli<sup>1</sup>

<sup>1</sup>Computer Science and Systems Engineering Laboratory, Department of Computer Science, Faculty of Science, Abdelmalek Essaadi University, Tetouan 93000, Morocco

<sup>2</sup>Department of Computer Science, Faculty of Science, Sidi Mohamed Ben Abdellah University, Fez 30000, Morocco

\*Corresponding author. E-mail: [yahya.mohammed@uae.ac.ma](mailto:yahya.mohammed@uae.ac.ma)

## Abstract

Brain imaging techniques play an important role in determining the causes of brain cell injury. Therefore, earlier diagnosis of these diseases can be led to give rise to bring huge benefits in improving treatment possibilities and avoiding any potential complications that may occur to the patient. Recently, brain tumor segmentation has become a common task in medical image analysis due to its efficacy in diagnosing the type, size, and location of the tumor in automatic methods. Several researchers have developed new methods in order to obtain the best results in brain tumor segmentation, including using deep learning techniques such as the convolutional neural network (CNN). The goal of this survey is to present a brief overview of magnetic resonance imaging (MRI) modalities and discuss common methods of brain tumor segmentation from MRI images, including brain tumor segmentation using deep learning techniques, as well as the most important contributions in this field, which have shown significant improvements in recent years. Finally, we focused in summary on the building blocks of the CNN algorithms used for image segmentation. In entire survey methodology, it has been observed that hybrid techniques and CNN-based segmentation are more effective for brain tumor segmentation from MRI images.

**Keywords:** segmentation methods, deep learning techniques, brain tumor segmentation, supervised segmentation, unsupervised segmentation, convolutional neural networks, segmentation architecture, magnetic resonance imaging

## 1. Introduction

Medical imaging techniques, such as positron emission tomography (PET), magnetic resonance imaging (MRI), computed tomography (CT), X-ray, and ultrasound have been widely employed for disease detection, diagnosis, and treatment during the last few decades. In clinical practice, MRI is particularly beneficial for evaluating gliomas, since it is feasible to obtain MRI sequences that provide complementary information (Bauer et al., 2013). Gliomas can be classified into high-grade gliomas (HGG) and low-grade gliomas (LGG), where the HGG are more offensive and infiltrative than the LGG (Bauer et al., 2013; Raschke et al., 2019).

Medical images are mostly interpreted by experts, such as radiologists. Practically, and due to the widely existing differences in the pathology and the possible fatigue of human experts, researchers and doctors have started to benefit from computer-assisted interventions. Although the evolution rate in the computation of medical image analysis has not been as rapid as that in medical imaging techniques, the situation is improving as deep learning techniques are introduced.

Image segmentation relies heavily on the effective extraction of important information and features from two-dimensional (2D) and 3D images. The objective of image segmentation is to segment an image into sole and exhaustive regions so that each region is spatially neighboring and the pixels inside the region are homogenous in terms of a pre-specified criterion, where the most

commonly used homogeneity criteria contain values of intensity, texture, color, range, surface normal, and surface curvature(s) (Bhandarkar et al., 1997). However, this description itself is one of the major restrictions of brain MRI images segmentation, especially when defining abnormalities tissue, since the tumors to be segmented are anatomical structures that are frequently flexible and complex in shape, highly variable in location and structure, and vary from patient to patient. Therefore, in the case of brain tumors, entails distinguishing between normal brain tissues (white matter; WM, gray matter; GM, and cerebrospinal fluid; CSF) and abnormal brain tissue (active tumor, edema, and necrosis tumor).

Brain MRI segmentation is a fundamental step in several applications of neurology, including quantitative analysis (Rabeh et al., 2017). MRI can properly define brain structures and provide a lot of information about anatomical soft tissues; however, MRI image segmentation is a difficult task due to limited spatial resolution, low contrast, intensity inhomogeneity (Tustison et al., 2010), and the difference in intensity range between the MRI sequences (Nyúl et al., 2000). Although many researchers have classified image segmentation techniques into many categories, there is no single typical segmentation technique that can yield acceptable results for different imaging applications. However, the aim of segmentation differs depending on the study purpose and the type of image data, where different techniques are used based on different conceptions about the natural of the images to be analyzed.

---

Received: July 31, 2022. Revised: December 16, 2022. Accepted: December 19, 2022

© The Author(s) 2023. Published by Oxford University Press on behalf of the Society for Computational Design and Engineering. This is an Open Access article distributed under the terms of the Creative Commons Attribution-NonCommercial License (<http://creativecommons.org/licenses/by-nc/4.0/>), which permits non-commercial re-use, distribution, and reproduction in any medium, provided the original work is properly cited. For commercial re-use, please contact [journals.permissions@oup.com](mailto:journals.permissions@oup.com)

Depending on the categorization strategy, segmentation techniques can be classified in a variety of ways:

- (i) Classification of the segmentation techniques into manual, semi-automatic and fully automatic (Ali et al., 2020; Meier et al., 2016; Moeskops et al., 2016; Pereira et al., 2016; Thaha et al., 2019) based on the degree of human interaction necessary in the segmentation of an MRI image (Wadhwa et al., 2019).

Manual segmentation refers to the process by which the radiologist segments and labels the image manually. In addition to the physiological and anatomical knowledge gained through training and experience, radiologists are required to master the multi-modality information provided by MRI images (Işin et al., 2016), where manual segmentation of brain tumors involves drawing the boundaries of the tumor manually and drawing the regions of anatomical structures with their various labels (Gordillo et al., 2013; Liu et al., 2014). Therefore, it is more sensitive to errors because it depends on human experts' intervention. The results of manual segmentation differ from person to person since it depends on the operator's knowledge and also demands a great deal of competence. Despite being a more time-consuming task, manual segmentation is the main method widely used to evaluate the accuracy of fully automatic and semi-automatic segmentation methods.

In semi-automatic brain tumor segmentation, human factor intervention is often required to initialize the method, verify the result accuracy, modify or manually correct the segmentation result, which results in effective segmentation. However, user intervention may yield diversity in segmentation results from a person to person. According to Gordillo et al. (2013) and Liu et al. (2014), the three main elements of the semi-automatic brain tumor segmentation method are the interactive part, user intervention is not required in fully automatic brain tumor segmentation. Instead, machine learning algorithms and prior knowledge are combined to make automatic segmentation. Knowledge of the location, size, shape, and expected appearance of the brain tumor is important for automatic methods and essential to have a model that not only describes the size, shape, and location but also allows adaptation for expected variations in features (Gordillo et al., 2013).

- (ii) Classification of the segmentation techniques into supervised (Bahadure et al., 2017; Naceur et al., 2018; Soltaninejad et al., 2018a) and unsupervised methods (Ilunga-Mbuyamba et al., 2016; Lok et al., 2017) based on manually labeled training data. Supervised methods use the labeled data in building the model which maps the extracted features to labels or classes in the training step, which are then utilized to select the label of data in the testing step (Wadhwa et al., 2019). The selection of correct training data is critical in supervised segmentation since different training data can lead to significant disparities during training, as well as possible discrepancies in segmentation results (Bezdek et al., 1993; Gordillo et al., 2013). Therefore, the training step demands human intervention, which ends in variable results. Supervised segmentation methods have the ability to limit manual intervention tasks by providing appropriate features, labeled data, and parameters that are appropriate to the learning algorithm.

In unsupervised segmentation, the processes of segmentation differ from supervised methods through the lack

of use of labeled training data. Therefore, the number of classes is determined automatically by an algorithm. The image is segmented into homogeneous regions using image-dependent features such as pixel intensity so that can deal with more complex conditions. Unsupervised segmentation methods are effective for handling more complicated cases, such as accurate segmentation of different tumor regions heterogeneous (Jiji & Ganesan, 2007).

- (iii) Conventional methods based on region-based (region growing and watershed) and thresholding-based (global thresholding and local thresholding) (Wong, 2005). Conventional methods are most commonly used as a first phase in the process of 2D image segmentation. The thresholding-based methods' idea is based on the postulate that the pixels belong to one class that falls within a certain range (Sujan et al., 2016). Region-based methods presume that a region is comprised of neighboring pixels that have similar properties (Bajwa et al., 2017; Sato et al., 2000).
- (iv) Classification of the segmentation methods based on deep learning techniques. Deep learning can be defined as a subset of machine learning, which has a network that is capable of learning from unstructured data, such as images and texts, and works in a similar way to the functioning of a human brain. A common key trait of deep learning methods is their focus on learning of data representations automatically (feature learning; Lundervold & Lundervold, 2019). This is the main difference between the deep learning approach and machine learning; in the deep learning approach, feature extraction and performing tasks are combined into one problem; thus, both are concurrently improved during the same training phase. See Lecun et al. (2015) and Hinton (2018) for an overview of the domain.

The unprecedented success of deep learning is mostly due to the advances in high-tech central processing units, graphics processing units (GPUs), the availability of a huge amount of data (big data), and the developments in learning algorithms. The proposed models of deep learning are typically trained and executed on specialized GPUs to reduce computation time. Technically, deep learning algorithms, especially convolutional neural networks (CNNs), have become a fast methodology for analyzing medical images (Sánchez et al., 2017) that have shown great improvement in traditional neural networks, which allows for building multiple-layer networks that can discover hierarchical feature representations such as higher level features that can be derived from lower level features (Lecun et al., 2015).

In recent years, deep learning has been involved in the segmentation of brain tumor images by using CNNs inside a more complex range to perform the segmentation due to its success in object recognition in 2D and 3D images. For this purpose, researchers have designed many CNNs architecture for brain tumor segmentation using MRI images in order to obtain more accurate results. Therefore, a number of these architecture have succeeded in segmenting large and small tumors of varying proportions. The methods used for segmentation are varied. On the one hand, several of the architecture have relied on automatic segmentation (Havaei et al., 2017; Kamnitsas et al., 2017b; Pereira et al., 2016; Thaha et al., 2019; Zhao & Jia, 2016), while on the other hand, some studies have used semi-automatic segmentation algorithms (Kwon et al., 2014; Hamamci et al., 2012; Havaei et al., 2015). These methods have achieved varying degrees of segmentation accuracy. This paper provides an analytical survey of the most popular methods that are used to segment the tumor in MRI

images. Despite the fact that the reference papers (Gordillo et al., 2013; Liu et al., 2014; Saman & Jamjala Narayanan, 2019; Wadhwa et al., 2019) provide detailed information on different segmentation methods with their disadvantages and advantages, there is still space for the contribution of the most recent methods, with a focus on using these methods thoroughly for brain tumor segmentation. In addition, this work is devoted to providing an abstract idea for deep learning techniques, specifically, the building blocks of CNNs that are used to segment the tumor in brain MRI images. It also presents researchers with new research directions for brain tumor segmentation in MRI images.

This survey is based on the largest number of papers and scientific research relevant to methods of brain tumor segmentation collected from several databases such as Scopus, Web of Science, Science Direct, IEEE Xplore, Springer, Frontiers, and Hindawi. In the selected databases, the inclusion and exclusion measures were applied to conference and journal papers published on brain tumor segmentation. Studies that did not meet the inclusion criteria (were duplicates, did not have access to the full text, or were not written in English) were not included. Figure 1 illustrates the search, inclusion, and exclusion process with the publication selection approach.

Initially, 698 publications were identified by scanning the selected databases and 25 publications were defined through cross-referencing. Following the elimination of duplicate publications, the remaining 573 papers were evaluated using exclusion criteria. Moreover, 324 publications were excluded after evaluating the title and abstract. The eligibility of 234 full-text research was examined, and 169 were selected for this study.

The remaining of this survey is organized as follows: In Section 2, we briefly present the modality of MRI. Then, Section 3 discusses the most relevant different brain tumor segmentation methods, including conventional methods, hybrid techniques, and deep learning techniques. Subsequently, we analyze the building blocks of the CNN algorithms used for images segmentation in Section 4. Finally, the survey conclusions are summarized in Section 5.

## 2. Magnetic Resonance Imaging

Brain tumor can be defined as a collection or mass of abnormal cells in the brain, which enclose the brain; any growth within such restricted space can cause problems. Brain tumors can be cancerous (malignant) or non-cancerous (benign). When benign or malignant tumors grow they can cause the pressure inside of skull to increase, and this can cause brain damage. The most common types of brain tumors are gliomas and meningiomas. Glial tumors are a type of brain tumor that arises from glial cells. It is a common and the most savage brain tumors, and most current brain tumor segmentation research focuses on providing detailed information about brain tumors.

Many medical imaging techniques such as MRI, magnetic resonance spectroscopy (MRS), CT, PET, and single-photon emission computed tomography are used to provide useful information about location, shape, and size. MRI is considered the standard technique widely used in the medical diagnosis of brain tumors. Moreover, the MRI has a significant impact on improved diagnoses, treatment planning, and growth rate prediction (Havaei et al., 2017).

MRI is one of the best and most common methods for evaluating patients with symptoms and signs that indicate a brain tumor. Its superior contrast accuracy allows it to assess tumor location and size, in planning appropriate treatment, and in eval-

uating treatment results. MRI modalities yield different types of tissue contrast images, therefore providing valuable structural information that can be used to diagnose and segment brain tumors. MRI includes four standard methods used to diagnose: "T2-weighted" MRI, "T1-weighted" MRI, "T1c-weighted" MRI with gadolinium contrast enhancement, and fluid attenuated inversion recovery ("FLAIR") (Drevelegas & Papanikolaou, 2011), and the structures of the brain tumor were segmented into edema, necrosis, and non-enhancing tumor (Fig. 2).

Generally, T1-weighted MRI was used to distinguish healthy tissues and necrotic cells, T2-weighted MRI was used to determine the region of edema, and FLAIR was used to cross-check the extension of edema and discriminate it, and suppressed the signal of water molecules which helps to differentiate the edema region from the CSF. Since necrotic cells do not interact with the contrast agent, the tumor boundary can be easily distinguished by the bright signal of gadolinium ions in the active cell region of the tumor tissue by T1c-weighted MRI (Menze et al., 2015). In the segmentation process, healthy tissue must be maintained so that it is not damaged during the stages of treatment.

## 3. Methods of Brain Tumor Segmentation

The main goal of image segmentation is to segment an image into homogeneous regions with respect to a predetermined standard. In the case of brain tumor segmentation, the tumor is segmented by separating the various tumor tissues from each other like edema, necrosis, and active tumor from normal brain tissue, such as CSF, GM, and WM.

There exist common segmentation methods used for obtaining the objective measure in order to define the homogeneity of each tissue during brain tumor segmentation. These methods can be divided into several categories as in Fig. 3 based on different principles such as the strategy of implementation, extent of user intervention, and the features used in each category; and provide the strengths and limitations of each subcategory as the Table 2 shows, namely conventional methods, supervised, and unsupervised segmentation methods, and segmentation techniques based on deep learning and hybrid methods.

### 3.1. Conventional methods

Conventional brain tumor segmentation methods are commonly used in 2D image segmentation and achieved more effective results in boundary drawing and segmenting the tumor region. Conventional methods include two standard image processing techniques, namely "thresholding-based" and "region-based" techniques (Gordillo et al., 2013).

#### 3.1.1. Thresholding-based technique

Thresholding-based segmentation technique is a fast, easy to implement, and effective conventional segmentation method by comparing their intensities with one or more intensity thresholds. The thresholding-based technique includes the "global thresholding" and a "local thresholding" (Gordillo et al., 2013; Liu et al., 2014; Saman & Jamjala Narayanan, 2019).

##### 3.1.1.1. Global thresholding

In the global thresholding method, the intensity is the best property that pixels in a region can share and depend it to determine the intensity ratio between objects and the background. The global thresholding is a suitable technique for an MR image that contains objects of similar contrast or high intensity between

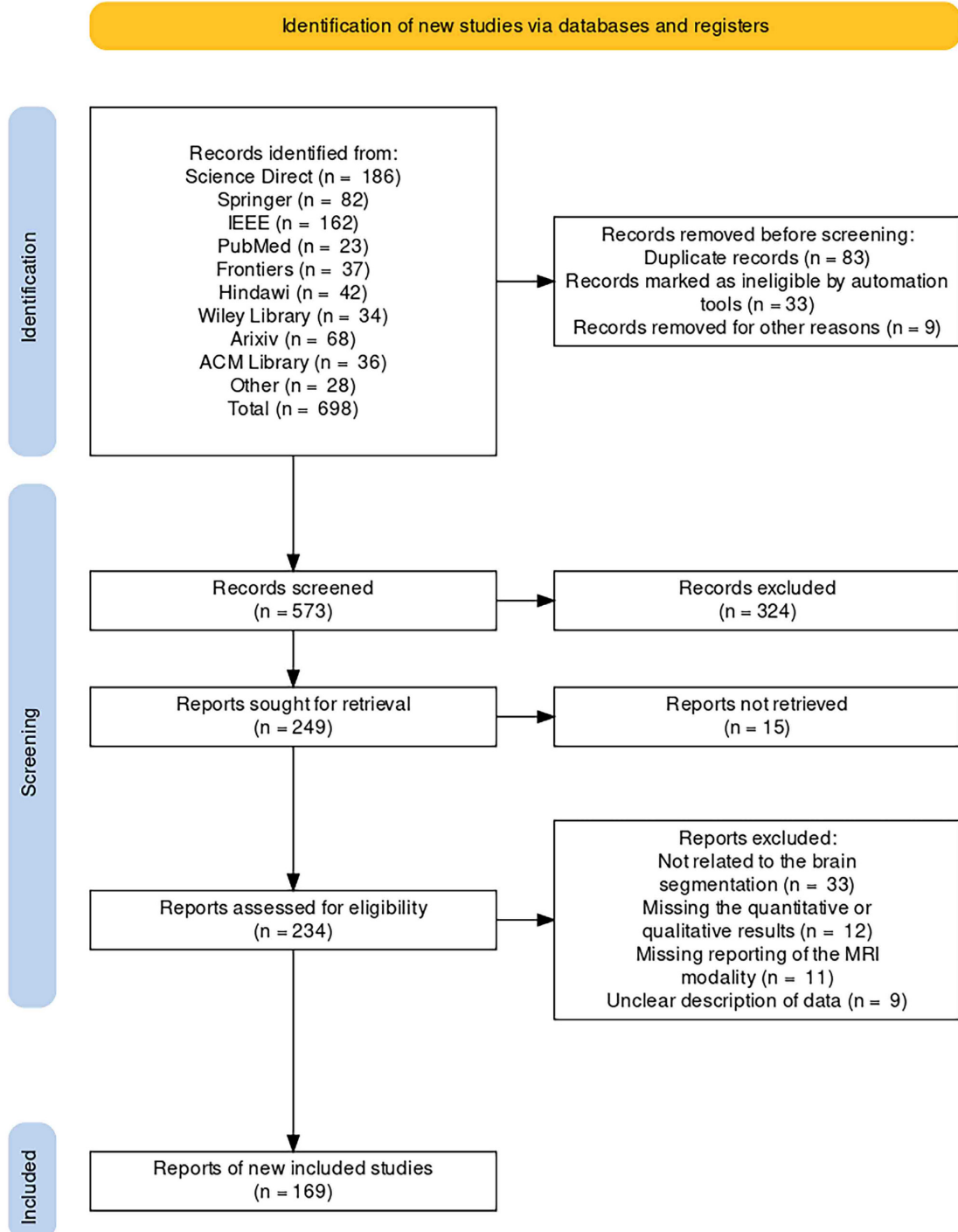


**Figure 1:** An overview of the process of collecting and selecting research on brain tumor segmentation methods according to PRISMA guidelines (Moher et al., 2010; Page et al., 2021).

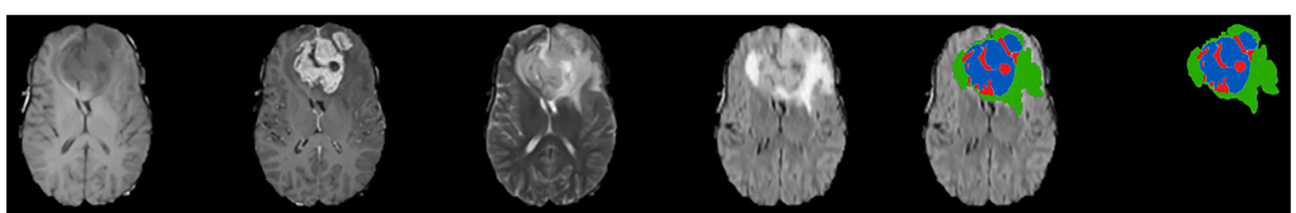


**Figure 2:** Brain tumor segmentation. From left: T1, T1c, T2, FLAIR, and segmented tumor. In segmented image, blue signal is an active region, red signal is necrotic core, and a green level signal is edema. Images are generated by using BraTS 2019 data.

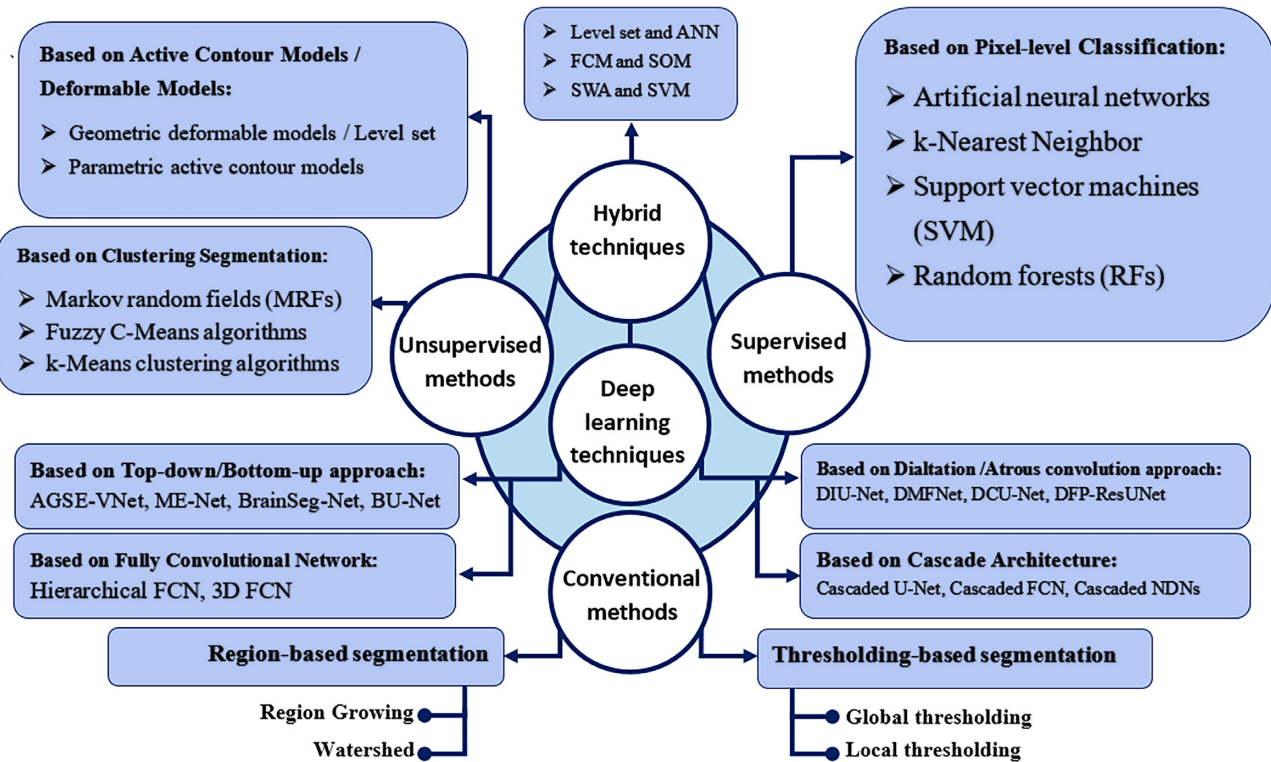


**Figure 3:** General methods and techniques for the segmentation of brain tumor images.

objects (Bhargavi & Jyothi, 2014; Ilhan & Ilhan, 2017). Mathematically, global thresholding technique can be defined by Equation (1). Where  $I(x, y)$  is an input image and  $f(x, y)$  be the thresholded version of  $I(x, y)$  and  $\tau = f(\{i \in I(x, y)\})$  is the threshold value.

$$f(x, y) = \begin{cases} 1, & \text{if } I(x, y) \geq \tau \\ 0, & \text{otherwise} \end{cases} \quad (1)$$

In global thresholding, the most common and computationally fast method for thresholding is to choose a single threshold value for the entire image. Thus, it is suitable for the segmentation of images containing objects with homogeneous intensity and does not contain any constant shape (Wong, 2005). In MR images, the major problem with the threshold method is that it focuses on intensity rather than the relationship between the pixels. Therefore, it may fail when two or more tissue structures have overlapping intensity levels.

### 3.1.1.2. Local thresholding

A local thresholding can be used effectively when a thresholding value cannot be determined from a histogram for the entire image and the gradient effect is small concerning the selected image size or cannot give better segmentation results by a single threshold (Bhargavi & Jyothi, 2014; Ilhan & Ilhan, 2017).

As shown in Fig. 5, the threshold value  $\tau_p$  depends on gray levels of  $I(x, y)$  and some local image properties of neighboring pixels (Saman & Jamjala Narayanan, 2019). Local thresholding method computes the threshold  $\tau_p$  for a pixel in a neighborhood  $N_p$  of a rather than from the entire image  $I(x, y)$ , local thresholding function  $\tau_p(x, y)$  is given in Equation (2).

$$f(x, y) = \begin{cases} 1, & \text{if } I(x, y) \geq \tau_p \\ 0, & \text{otherwise} \end{cases} \quad (2)$$

where  $\tau_p = f(\{i \in N_p(x_p, y_p)\})$

### 3.1.2. Region-based techniques

Region-based segmentation techniques examine pixels in an image and form disjoint regions by integrating the neighborhood pixels with homogeneity properties based on a predefined similarity standard. The region-based technique includes "region growing" and "watershed".

#### 3.1.2.1. Region growing

The region growing is a popular region-based segmentation technique used to extract a homogeneous region from an image includes collections of pixels/voxels that have the same intensity values (Adams & Bischof, 1994; Haralick & Shapiro, 1985). Region growing requires the starts with a seed point that belongs to the region of interest (ROI), then all neighboring pixels are checked to ensure their intensely satisfied the similarity criteria then added to the growing region. The growing process is repeated gradually until no more pixels/voxels can be added to the growing region as in Fig. 4.

Region growing is effectively used in medical image analysis to segment different tissues, tumors, or lesions from MR images. Therefore, many experiments (Salman et al., 2005a, b) have demonstrated that region growing is an efficient and computationally less complex approach than other methods for brain tumor segmentation, especially for tissues and homogeneous regions. Kaus et al. (2001) used a region growing technique that involved the repetition of statistical classification for segmenting MR images of brain tumors into several tissue classes based on the signal intensity value, where tissue classes were specified on the classified images with region growing segmentation operations.

The advantage of the region growing technique is that it is capable of correctly separating regions of similar intensity. The partial

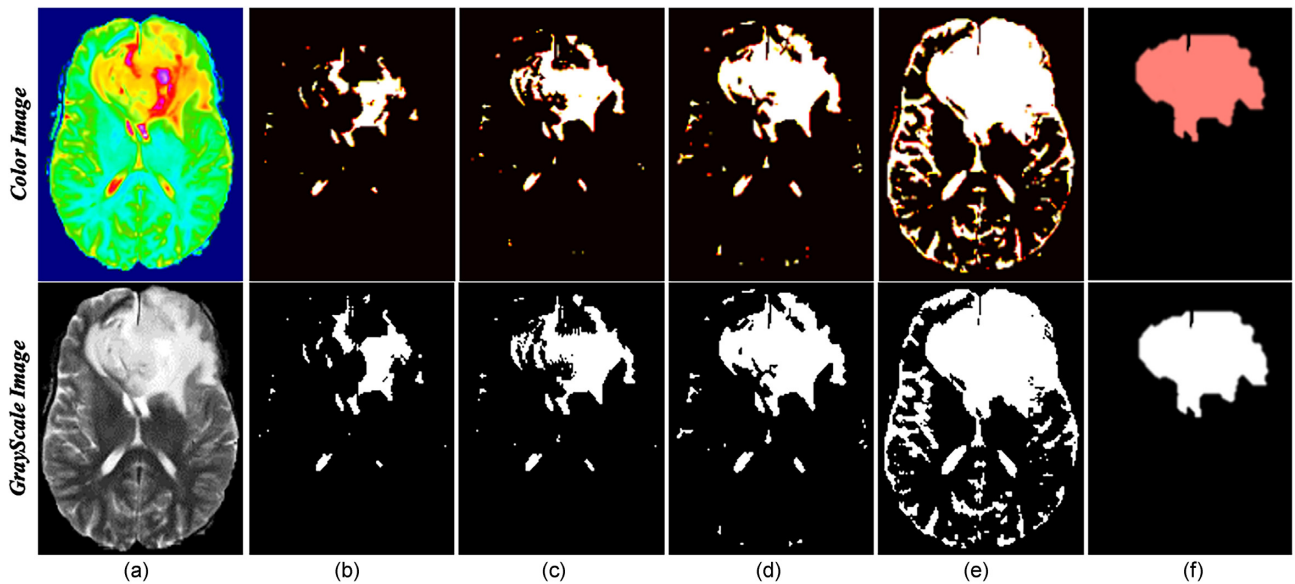


**Figure 4:** A region growing segmentation of a brain tumor. From left: (a) an MR image (T2 modality) of a human brain tumor, (b) the seed point is selected manually or randomly using the seeded region growing (SRG) algorithm (Adams & Bischof, 1994), (c) a partial segmentation into several seed classes, (d and e) gradually expanding the growth region to include all neighboring pixels that contain soft tissue, CSF, GM, and WM, and (f) completed segmentation is obtained that denotes only the tumor region.

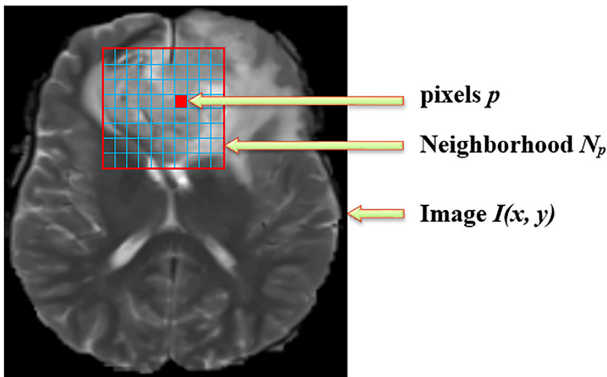


**Figure 5:** Illustrated the method of computing local thresholding, the threshold for a pixel is based on the intensity statistics of a local neighborhood rather than the entire image.

volume effect is one of the problems of the region growing technique; it limits the accuracy of MR image segmentation by blurring the intensity between tissue classes at the border of the two tissues types, thus making the one voxel represent different types of tissue (Sato et al., 2000). This problem is overcome by the introduction of the modified region growing method (Lakare, 2000), which worked to remove the partial volume effect by using the gradient information to define the boundaries more accurately.

### 3.1.2.2. Watershed

Watershed segmentation is one of the region-based techniques that utilize image morphology. The idea of a watershed comes from the behavior of water in landscapes. The drops of water falling during the rain will collect in catchments basins in different regions according to the amount of water. These basins are associated with different valleys (each valley is related just to a catchments basin), and each point in the landscape belongs just to one unique basin.

The water will pour into each catchment and start to fill the valleys. However, the water from different catchments is not allowed to mix. Thus, dams are built at the points where the water coming from the different basins meets. These dams are the boundaries watersheds (Kuo et al., 2008). The image represents landscapes where the bright pixels represent mountaintops, the dark pixels represent valleys, and dams also represent the boundaries of image objects. Figure 6 shows the details of the watershed technique, where each object in the image has different boundaries that distinguish it from the rest of the objects. More description about the watershed technique can be found in references (Preim & Botha, 2014; Rogowska, 2000).

Watershed technique has been commonly used for MR brain tumor segmentation; user-based hierarchical watershed technique of brain tumors from MRI data was evaluated by Cates et al. (2005). In comparison to manual segmentation, both quantitative and qualitative results demonstrated improvements in segmentation time and accuracy, with equivalent visual and statistical quality. The study also discovered certain flaws in the watershed technique, such as edges in the data that were poorly defined, and a trend in the hand-segmentation results toward consistently bigger segmentations. The analysis concluded by casting questions about the usefulness of utilizing expert segmentations to determine ground truth.

According to Li et al. (2007), the oversegmentation problem yet persists in this technique. Some pre-processing or post-processing approaches have been suggested to avoid oversegmentation (Gies & Bernard, 2004), resulting in a more feasible segmentation that reverses the shape of objects (Bleau & Leon, 2000). For the segmentation of brain tumors, Bhattacharya and Das (2008) used a marker-based enhanced watershed method based on the previous knowledge of the test images.

Ratan et al. (2009) presented a simple supervised and image-based technique of MRI brain image analysis that requires very little computational power. It is a watershed segmentation-based method for tumor detection in 2D and 3D brain MRI.

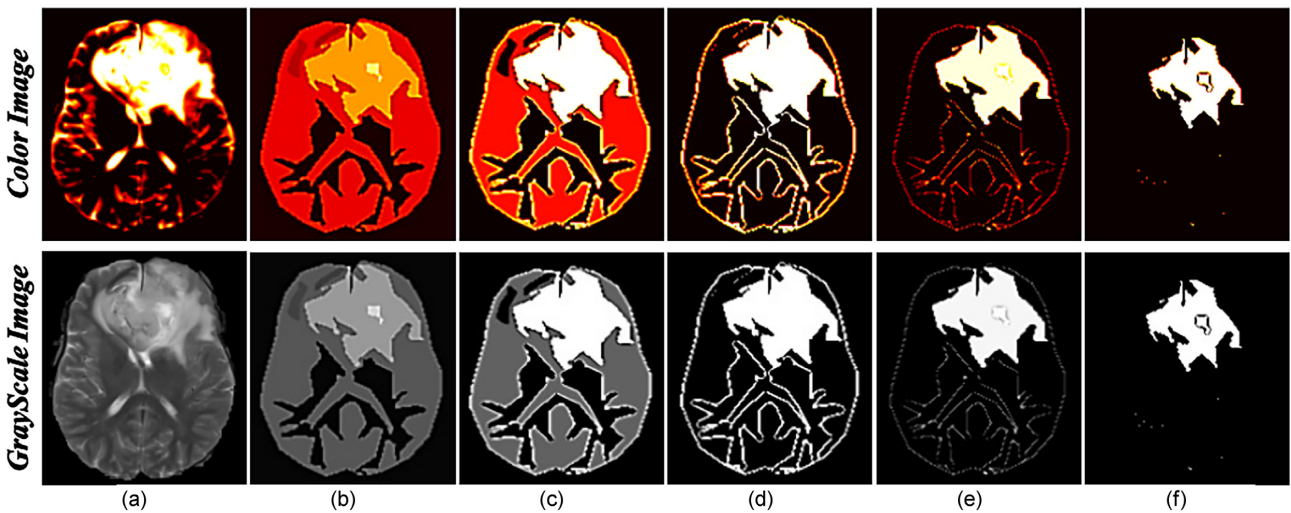


**Figure 6:** Image segmentation using the watershed technique. (a) Original image T2 modality for a brain tumor, (b) result of a watershed segment operation performed on the original image, and (c, d, and e) expanding the watershed of the region growing in order to obtain the bright pixels that represent the final segmentation in the image (f).

Finally, the successful results of brain tumor segmentation using conventional methods are difficult to accomplish. These methods have been used as a pre-processing step in the segmentation of the brain tumor in the majority of cases. Consequently, more advanced automatic techniques have been suggested to meet the needs of clinical practitioners.

### 3.2. Supervised methods

Supervised segmentation methods are used with labeled training data. Supervised segmentation includes both a training phase that uses labeled data to build a model that extracts features to labels or classes (where human intervention is required in this phase that finishes up with variability of results), and a testing phase that is used to specify labels to unlabeled data based on the measured features.

The goal of supervised segmentation methods is to infer a functional connection from training data that are well generalizable to testing data; the connection takes the form of a series of equations with numerical coefficients or weights (Liu et al., 2014). The selection of appropriate training data is crucial in the supervised method of segmentation since various training sets can lead to significant changes in training time as well as possible discrepancies in segmentation results (Bezdek et al., 1993).

A key benefit of employing the supervised segmentation techniques is being able to accomplish different tasks simply by altering the training set. As well, it has can reduce the manual engineering task by supplying features and parameters that are appropriate to the learning algorithm. The details of supervised learning-based approaches are cited in reference (Soltaninejad et al., 2018a) for a better understanding.

When working out the brain tumor segmentation task as a supervised segmentation problem, one simple method is to use the labels normal and tumor as classes and to use the intensity in the various MRI images as features (Gordillo et al., 2013). Several researchers have classified supervised segmentation techniques and discussed as follows:

#### 3.2.1. Segmentation based on pixel-level classification

A classification technique based on pixel-level is a supervised segmentation method that specifies an image feature space using

data with known labels, which requires the segmentation of images used for training manually and then used as benchmarks for the automatic segmentation of new images. Image features are typically the intensity of pixels and values, where the pixels of an image can be represented in the space of the features using the different pixel attributes.

The disadvantage of the supervised classification techniques is that they may lead to skewed results when using the same training set for a large number of images, also ignoring local information makes it more sensitive to noise. In brain tumor segmentation, most commonly used supervised classification techniques in the literature are ANNs, k-NN, RF, and SVM.

##### 3.2.1.1. Artificial neural networks

ANN is a segmentation technique based on the neural network, usually is trained or fed a significant quantity of data through a series of nodes when it is first created, where each pixel is represented by a neuron (Kang et al., 2009). Training involves providing the input and training the neural network for knowing the connections and weights between the nodes and instructing the network on how to produce the desired output. The known features are fed into input nodes and mathematical processes are performed on them in order to develop a final classification.

Feature extraction is the first step in ANN; features are extracted from images in such a way that they may be used as input for segmentation and next step is image segmentation. The connection between hidden nodes and output layer is classified into a feed-forward neural network (Kavitha et al., 2012; Wang et al., 2015), a feed-back propagation neural network (Dilruba et al., 2006; Schmidl et al., 1993; Sornam & Devi, 2015), and a radial basic function (Montazer & Giveki, 2015).

A specific kind of ANN that has been broadly used in visual pattern detection is the self-organizing map (SOM; Vijayakumar et al., 2007), which is a popular case of ANN introduced by Kohonen (1982) with the automatic topological mapping process. The process of topological mapping that the SOM offers makes segmentation images more appealing than other ANN. The SOM can maintain the topological changes in the image by using a different neighborhood procedure (Sandhya et al., 2020).

The advantage of neural network-based segmentation techniques is the ability to model distributions and non-linear dependencies, segmentation effectiveness for non-regular datasets, better computational capabilities, and low expert-intervention needs during segmentation (Tripathi et al., 2018).

### 3.2.1.2. K-nearest neighbor

The k-NN algorithm is a very simple, easy to implement classification-based segmentation technique. The idea of k-NN is based on segregated pixels (voxels in 3D images) which are categorized into classes based on their correspondence with the features of a set of similar pixels that exist near each other, where the nearest unlabeled neighbor is performed, then the class or label is determined using those neighbors. In order to predict the label of test points, the similarity or distance between the training cases and the new unlabeled test points is estimated (Cunningham & Delany, 2020). This classification technique has great relevance since with the current processing capacity, concerns about poor runtime performance are no longer a concern.

Warfield et al. (2000) used the k-NN classification algorithm for brain MRI segmentation. They developed k-NN statistical classification based on MR intensity; however, because the image contains overlapping MR intensity areas, this technique is unable to segment tumor structures. Ramteke and Monali (2012) presented automatic classification and abnormality detection from CT scan brain images by using a k-NN classifier. The statistical texture feature set is derived from normal and abnormal images. The k-NN classifier was applied for classifying image and achieved good results compared to the SVM classification rate.

### 3.2.1.3. Random forest

RF is a simple supervised classification approach that runs most effectively with huge datasets. It is relatively robust with respect to noise, supports more input variables without variable loss, and considers significant classification features. According to Breiman (2001), "a random forest (RF) is a classifier consisting of a collection of tree-structured classifiers  $\{h(\mathbf{x}, \Theta_k), k = 1, \dots\}$  where the  $\{\Theta_k\}$  are independent identically distributed random vectors and each tree casts a unit vote for the most popular class at input  $\mathbf{x}$ ".

In the case of brain tumor segmentation, RF is the most effective method for dealing with high-dimensional feature vectors, multi-class classification issues, and HGG. Koley et al. (2016) used RF for pattern classification after identifying and extracting the tumor region. The extracted lesions have been quantified with 86 different characteristics being used to develop the training dataset, which is subsequently fed into the classifier. Goetz et al. (2016) presented a novel RF-based approach that relies on a technique called domain adaptation in order to decrease sample selection errors induced by sparse sampling. The suggested technique uses sparse and unambiguous annotations to generate high-quality classifiers for various tissue classes. Soltaninejad et al. (2018b) suggested a learning-based technique for automated brain tumor segmentation in MRI images, in which the MRI image voxels are classified into normal brain tissues and various regions of tumors using RF. The patient overall survival time task was predicted using volumetric characteristics of segmented tumor tissues and patient age applied to a regression-based RF. The method effectiveness was evaluated on MICCAIBraTS 2017 challenge dataset.

### 3.2.1.4. Support vector machine

SVM was used as a kernel-based parametric approach for treating supervised classification issues (Vapnik, 1999). It can be especially

useful for multi-domain classification applications and present a robust technique for binary classification. However, implementing the SVM is both computationally expensive and theoretically mathematically complex (Suthaharan, 2016). Because of its high classification capacity, SVM has been commonly employed in the domain of brain tumor segmentation. SVM enables detection and localization of brain tumors in MRI, as well as segmentation of the tumor cells to know the size of the tumor in that segmented region (Sathies Kumar et al., 2017). To find the optimal hyper-plane to better classify the data, SVM is working to split the image into two classes by selecting the hyper-plane which has the largest distance from each nearby data point (Ayachi & Ben Amor, 2009; Yang et al., 2016) as given in Fig. 7. The optimization issue must be solved as follows:

$$\min \frac{1}{2} \mathbf{w}^T \mathbf{w} + \rho \sum_{i=1}^n \varepsilon_i \quad (3)$$

subject to  $y_i(\mathbf{w}^T \phi(\mathbf{x}_i) + b) \geq 1 - \varepsilon_i$  and  $\varepsilon_i \geq 0$ . The instance-label pairings of the provided training dataset are denoted by  $\{(\mathbf{x}_i, y_i), \dots, (\mathbf{x}_{n-1}, y_{n-1}), (\mathbf{x}_n, y_n)\}$ ,  $i = 1, 2, \dots, n$  and express the hyper-plane by  $(\mathbf{w}, \mathbf{x}_i) + b = 0$ , where  $(\mathbf{w}, \mathbf{x}_i) \in \mathbb{R}^n$  and the offset of the hyper-plane  $b \in \mathbb{R}$  is real. The standard vector of separating hyper-plane is  $\mathbf{w}$ , slack variables were computed for soft margins in the non-separable case via  $\varepsilon_i = 1, 2, \dots, n$  and a penalty parameter for the error term  $\rho$ . In addition, SVM transforms the data into a higher dimensional feature space using a kernel function  $K(\mathbf{x}_i, \mathbf{x}_j) = \phi(\mathbf{x}_i)^T \phi(\mathbf{x}_j)$ , allowing the data to be linearly separated with a maximum margin (Bauer et al., 2011).

Sandabadi et al. (2016) proposed a method for detecting and segmenting brain tumor regions in T1-weighted MRI. The method has three main steps, one of these steps is tumor detection and classification using SVM into two classes: tumor and no-tumor class.

Using one-class SVMs, Zhou et al. (2005) proposed a segmentation technique for brain tumor extraction from MR images. In addition to superior segmentation results for brain tumor extraction compared to fuzzy clustering technique, the proposed technique can learn the non-linear distribution of images based on one-class SVM without previous knowledge via the automated procedure of SVM parameters training and an implied learning kernel.

Based on a genetic algorithm (GA) and an SVM, Kharrat et al. (2010) used a hybrid approach for extracting the optimal brain tissue features based on the spatial gray level in MRI and solved the selection features by GA, and gave extracted features as input to SVM for classifying tissues into a normal, malignant, or benign tumor.

### 3.2.1.5. Superpixel-based segmentation

The superpixel technique aims to cluster similar pixels with low-level properties to create visually meaningful entities (Stutz et al., 2018), in which the image is segmented by using a technique called simple linear iterative clustering (SLIC) to create tiny regions known as superpixels (Achanta et al., 2012). Therefore, superpixels are computationally efficient due to reducing the complexity of the huge number of pixels in an image to just a few superpixels (Fig. 8; Wang et al., 2017b).

Superpixel segmentation algorithms have been segmented into several types according to various classification benchmarks. For instance, Achanta et al. (2012) classified superpixel algorithms into graph-based and gradient-ascent-based methods depending on the iterative process. Xu et al. (2014) classified the superpixel segmentation strategy into bottom-up and top-down algorithms based on the generating saliency-based superpixels

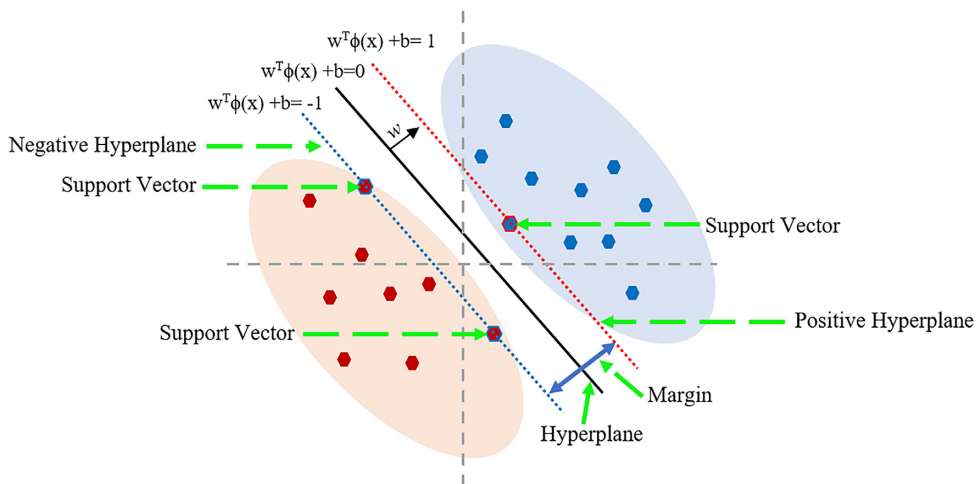


**Figure 7:** Using SVM to split a set of images into two different classes. The classification is done by getting the hyper-plane based on a kernel function ( $K$ ) that separates the two classes.

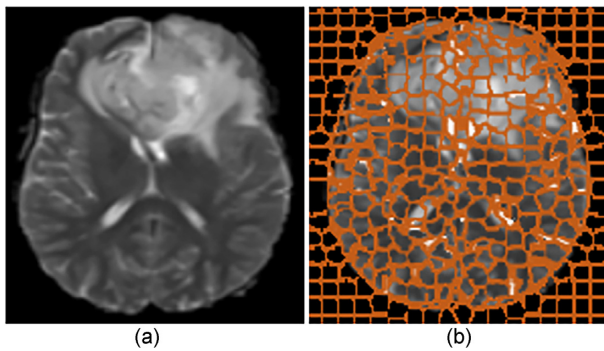


**Figure 8:** Superpixel segmentation. (a) Original image (T2 modality) and (b) superpixels generated for the original image.

method. Wang et al. (2017b) classified superpixel algorithms into two categories: graph-based and clustering-based methods, according to a view of the segmentation model.

Superpixels have been employed in brain tumor segmentation from MRI images as an efficient approach to minimize the number of image primitives subsequently required for further processing, in which the researchers have significantly improved the superpixels approach to obtain more effective segmentation results (Alipour & Hasanzadeh, 2021; Imtiaz et al., 2020; Soltaninejad et al., 2017; Su et al., 2013).

Su et al. (2013) designed the graph spectral clustering algorithm to classify the superpixels into different categories, including necrosis and enhanced tumor based on MRI images. The local  $k$ -means clustering approach is used to create superpixels by segmenting the MRI images into a number of homogenous regions. Alipour and Hasanzadeh (2021) used SLIC to generate superpixels, which are used as atomic units for more procedures in subsequent operations to reduce the sensitivity and computational cost. Consequently, the generated superpixels have regular forms, especially in regions with the existence of noise and non-homogenous in MR images.

Soltaninejad et al. (2017) proposed a fully automated approach for brain tumor segmentation from MRI images based on the superpixel technique and classification of each superpixel. For guarantee robust classification, a number of image features are computed from each superpixel within the whole brain region in FLAIR

MRI images including intensity-based, curvatures, Gabor textons, and fractal analysis.

Imtiaz et al. (2020) presented an approach for brain tumor segmentation based on superpixel-level features extracted from 3D MR images. In this method, each image is segmented into irregular patches called “superpixels” based on its intensity and spatial similarity. This is done to avoid randomness pixels and to account for the non-homogeneous fine boundaries of brain tumors.

### 3.3. Unsupervised methods

Unsupervised methods do not rely on manually labeled training data; instead, the homogenous features together can be grouped and numerous classes decided automatically by an algorithm that groups similar pixels. In unsupervised segmentation methods, the image is split into the homogeneous area by utilizing image-based characteristics like pixel intensities. These techniques can deal with more complex cases; for instance, generating a precise segmentation of the various areas present in a heterogeneous tumor into distinct areas (Jiji & Ganeshan, 2007). To assess segmentation quality, unsupervised segmentation may be conducted using either an anatomical objective measure or an image-based objective measure. Image segmentation is based on the evaluation of regions with similar intensities or textures in image-based objective (Gordillo et al., 2013).

Since it is difficult to translate the visible processing and anatomical knowledge that specialists use into processes that yield the required results, most of the unsupervised methods of brain tumor segmentation have focused on the segmentation of enhancing tumor regions (tumor or edema). This type of segmentation is more difficult because of the lack of previous shape or label for the tumor (Popuri et al., 2009). The unsupervised methods of segmentation are classified as follows:

#### 3.3.1. Clustering-based segmentation

Clustering-based segmentation is a type of unsupervised method for segmenting unlabeled image data into clusters of pixels/voxels keeping similar intensities that share some features in same cluster and dissimilar pixels in different clusters (Wadhwa et al., 2019). The clustering method can be divided into two categories, namely hard clustering and soft clustering (Bora & Gupta, 2014, 2015). In hard clustering, one pixel/voxel can belong to one cluster only of pixel/voxel that has the same features and intensity. But in soft

clustering, the result provided is a probability of a pixel/voxel belonging to two or more of the defined clusters.

### 3.3.1.1. Density-based clustering

Density-based clustering is created based upon the density of the pixel/voxel which is represented in the image region. The regions that become dense due to a large number of pixels similar in that region are considered clusters. Density-based clusters are separated from each other by contiguous regions of a low-density of pixels (Campello et al., 2020). The pixels found in low-density regions are commonly referred to as noise or outliers. The density-based clustering algorithms are classified as follows:

- (i) Hierarchical density-based spatial clustering of applications with noise (HDBSCAN): HDBSCAN (Campello et al., 2013) generates a complete density-based clustering hierarchy that allows extracting a simplified hierarchy consisting just of the most significant clusters.
- (ii) Density-based spatial clustering of applications with noise (DBSCAN): DBSCAN (Daszykowski & Walczak, 2009; Ester et al., 1996) can only provide data objects based on a global-density threshold in flat-label non-hierarchical, which means DBSCAN collects data points based on both the distance metric "Eps" and a minimum amount of data points called "MinPts" (Ester et al., 1996). However, a single density threshold often cannot correctly distinguish common data clusters with clusters of very different densities or overlapping clusters.
- (iii) Ordering points to identify clustering structure (OPTICS): OPTICS (Ankerst et al., 1999) is a cluster analysis method that uses a density-based approach but does not construct a clustering of data objects explicitly. Instead, it provides an enhanced ordering of the data that represents its density-based clustering structure. OPTICS only proposes how to extract a flat division by applying a global-density threshold, which may not lead to the most significant clusters if these clusters have varying densities. In addition, OPTICS worked to discover the data structure by separating data objects according to the reachability distance RD and core distance CD, in which the neighborhood radius of an object may be defined by the core distance to its nearest neighbor (Daszykowski & Walczak, 2009).

### 3.3.1.2. k-Means clustering

The k-means clustering is a basic technique in pixel-based methods (Vijay & Subhashini, 2013; Wadhwa et al., 2019) that splits the input data into  $k$  clusters based on the distance metric used for the clustering in which the resulting intra-cluster similarity is big but the inter-cluster similarity is low, then mean intensity for each cluster is continually calculated and partitions the image by classifying each pixel/voxel in the cluster to with the nearest centroid (Kang et al., 2011).

The k-means clustering is a very computationally expensive algorithm and can also incorrect and poor results in the case of improper selection of  $k$  value (Pham et al., 2005; Saman & Jamjala Narayanan, 2019) because it calculates the distance of every data point for all clusters at each repetition with the centroids. The goal of this method is to minimize an objective function as Equation (4):

$$J = \sum_{j=1}^k \sum_{i=1}^n \|x_i^{(j)} - C_j\|^2, \quad (4)$$

where  $J$  is objective function,  $\|x_i^{(j)} - C_j\|^2$  is a chosen distance measure between a data point  $x_i^{(j)}$  and the centroid for cluster

$$C_j = \frac{1}{N_j} \sum_{x \in x_j} x, j = 1, 2, \dots, k$$

$k$  is a number of clusters, and  $n$  is an indicator of the distance of the data points from their respective cluster centers.

In MR brain images,  $k$ -means have been used to separate the position of tumorous tissues from the healthy ones by converting gray-level MR image into RGB image to enhance its features by applying pseudo-color transformation (Wu et al., 2007). The same idea was implemented by Juang and Wu (2010) on MRI brain lesion images for tracking tumor to help specify exactly the size and region of the lesion and the approach gave very hopeful results.

Alam et al. (2019) proposed a method that combines the template-based  $k$ -means and enhanced FCM algorithm for identifying human brain tumors in an MRI image in which the template-based  $k$ -means method is used to greatly improve segmentation by selecting the ideal template based on image gray-level intensity. The results showed that the suggested approach achieves better detection of normal and abnormal tissues in the human brain under modest detachment of gray-level intensity. Furthermore, compared to previous methods, this approach detects brain tumors in a very short time.

Liu and Guo (2015) have proposed a strategy based on  $k$ -means clustering technique and SVM to segment brain MRI image, which used  $k$ -means clustering to get the initial classification result as the class label and select the feature vectors for each pixel of the brain tissue as training and test samples. The results showed that the suggested segmentation technique achieves a better segmentation effect.

### 3.3.1.3. FCM clustering

FCM clustering is the most important and well-known method that has been widely used in MRI (Balafar, 2014), where the pixels in the image are classified into multiple classes (Yang & Fei, 2011) by assigning membership for each of the pixels units corresponding to each class center on the basis of the distance between the classes and the pixels units, where each pixel can belong to two or more classes. Another benefit of the FCM technique is adaptability when dealing with data having multiple cluster solutions since fuzzy membership functions are used (Ganesh et al., 2017). The objective function of FCM is calculated applying the equation

$$J_m = \sum_{i=1}^n \sum_{j=1}^c (u_{j,i})^m \|x_i - C_j\|^2. \quad (5)$$

Compared to  $k$ -mean clustering, FCM gives comparatively better results with overlapped pixels, in which FCM divides the image data into fuzzy centers clusters  $C_j$  using the below equation:

$$C_j = \frac{\sum_{i=1}^n x_i (u_{j,i})^m}{\sum_{i=1}^n (u_{j,i})^m}, \forall j = 1, \dots, c \quad (6)$$

where  $C_j$  represents the  $j^{\text{th}}$  cluster center,  $u_{j,i} = u_j(x_i)$  represents the fuzziness membership between  $[0, 1]$  of  $i^{\text{th}}$  pixel to  $j^{\text{th}}$  cluster center,  $n$  is the number of pixels,  $m$  is the fuzziness index  $m \in [1, \infty]$ , and  $c$  represents the number of cluster center. The following

equation can be used to calculate fuzzy membership  $u_{j,i}$ :

$$u_{j,i} = \frac{1}{\sum_{k=1}^c \left( \frac{\|x_i - C_j\|}{\|x_i - C_k\|} \right)^{\frac{2}{m-1}}}, \quad (7)$$

where  $x$  are pixels of image and  $C_j$  and  $C_k$  are cluster point.

FCM algorithm for segmenting brain tumors is becoming a very popular technique and fruitful research field, in which the FCM algorithm worked to solve the issue of identifying the homogeneity features that may not have sharp transitions at region boundaries. In brain tumor segmentation, the FCM clustering algorithm has shown encouraging results through tumor segmentation into multiple tissue classes using different membership classes including active cells, necrotic core, and edema (Liu et al., 2014).

Setyawan et al. (2018) used the FCM algorithm to examine the effect of pre-processing stages to segment the MRI image especially to detect brain tumors by the technique of opening and closing morphology that is used to connect the pixels adjacent, where it can reduce the noise in the image in order to classified regions to become connected. Yang and Fei (2011) presented a method to achieve accurate MRI brain classification by improving the intensity of the image using a modified multi-scale and fuzzy c-means. The method used a bilateral linear filter to reduce noise in MR images and processes the degradation of image contrast and detail by incorporating a partial edge detection track into the filtering to support intra-region smoothing and preserve the inter-region edge. In addition, the method used a multi-scale image series by increasing the standard deviation of the spatial function and lowering the standard deviation of the range function.

Ganesh et al. (2017) proposed a clustering method named enhanced adaptive fuzzy k-means (EAFKM) that is used to segment the MRI brain image into three various subregions: CSF spaces, GM, and WM. The result is then compared with the FCM and adaptive fuzzy k-means (AFKM) algorithms. The EAFKM clustering method is an improvement over the AFKM clustering algorithm proposed by Quteishat et al. (2013), which is a combination of FCM clustering, moving k-means, and K-means clustering (KM) to demonstrate that MRI brain images can be classified and segmented better than the traditional method. The featured EAFKM can supply a better and more adaptive clustering process in which the image looks clearer when compared to the traditional methods of FCM and AFKM. All the results of the EAFKM algorithm yielded better results compared to the FCM clustering and AFKM.

### 3.3.1.4. Markov random field

The MRF approach was first suggested by Besag (1975), which was later developed for image processing applications (Geman & Geman, 1984). A wide assortment of approaches based on MRF has been suggested for image segmentation, specifically MRI brain segmentation (Ahmadvand et al., 2017; Marroquin et al., 2002; Yousefi et al., 2012). The MRF approach is an effective technique for merging image features, including context, intensity, texture, spectral properties, and spatial information into the clustering process. This method is commonly used in image segmentation as a probabilistic approach to reduce the likely problem of overlapping and the noise effect on the clustering result (Tran et al., 2005).

MRF provides a simple and effective technique to represent spatial dependencies in image pixels. As a result, it is utilized to model the relationship between neighboring pixels. In the instance of brain tumor segmentation, the region is strongly classified as a brain tumor or non-tumor, and then MRF evaluates if

the neighboring pixels have similar properties belong to the same region (tumor or non-tumor) as Fig. 9. Conditional random fields (CRFs) have been presented as a method to develop probabilistic models to segment and label sequence data (Lafferty et al., 2001).

The MRF and CRF algorithms are capable of representing complicated dependencies among data instances, which gives high precision in brain tumor segmentation tasks (Lee et al., 2005). As a result, these approaches are increasingly being used in various segmentation tasks.

The label field  $\Omega$  on lattice  $\mathbf{S}$  is known to be an MRF, if and only if, two below conditions are valid:

$$P(\omega_s|\omega_r, r \neq s) = P(\omega_s|\omega_r, r \in N_s)$$

The first condition is known as positivity and the second is known as Markovianity, where  $r$  demonstrates all sites of the lattice  $\mathbf{S}$ , and  $N_s$  represents the neighbors of the pixel  $s$ .

The energy function has to be defined in hidden states corresponding to true values of each pixel, and then reduced to get the best prediction. The energy function is defined as below:

$$U(\omega_s) = \sum_s \left( \log(\sqrt{2\pi} \sigma_{\omega_s}) + \frac{(f_s - \mu_{\omega_s})^2}{2\sigma_{\omega_s}^2} \right) + E(\omega), \quad (8)$$

where  $E(\omega) = \sum_{s,r} \beta \delta(\omega_s, \omega_r)$ . The purpose of the MRF is to discover the minimum energy function in the pixels of the possible label field's space.

In order to overcome the MRF drawbacks, Ahmadvand et al. (2017) proposed a unique solution based on a good combination of MRF model and watershed technique. The results illustrate that the suggested technique is successful in MRI image segmentation and effectively reduces computational time. The oversegmentation result obtained by the watershed algorithm is processed using the region adjacency graph (RAG). The watershed-MRF technique is then applied to RAG for the produce of initial segmentation, in which boundaries are disregarded due to the complicated boundaries in MRI images. Thus, a small percentage of pixels are chosen to represent the real boundaries of tissues and then are labeled using the watershed-MRF technique that has been adjusted to merge pixels and regions.

Capelle et al. (2000) proposed an unsupervised method using an MRF model that statistically used the impacts that neighboring pixels should have on each other's labels, eliminating the necessity for morphological procedures. The proposed method used MRF to model the segmentation field that contained the classification of each singular pixel with the iterated condition modes algorithm.

For segmentation of single and multi-spectral MRI images in real-time environments, Yousefi et al. (2012) have proposed a novel approach based on a hybrid of MRF and social algorithms that include a gossiping algorithm and an ant colony optimization (ACO). Merging ACO with the gossiping algorithm allows the discovery of a better track based on neighborhood information. As a result of this interaction, the algorithm converges to an optimal solution faster.

### 3.3.2. Active contour models/deformable models

The most previous mentioned segmentation methods have achieved great success in segmenting the 2D MRI images for the extraction of brain tumor boundaries. Model-based segmentation techniques are mostly used in 3D image segmentation (Chang & Valentino, 2008) as geometric deformable models and parametric deformable models, in which a linked and continuous model for a certain anatomic structure is constructed by incorporating prior knowledge of the object like shape, location, and orientation.

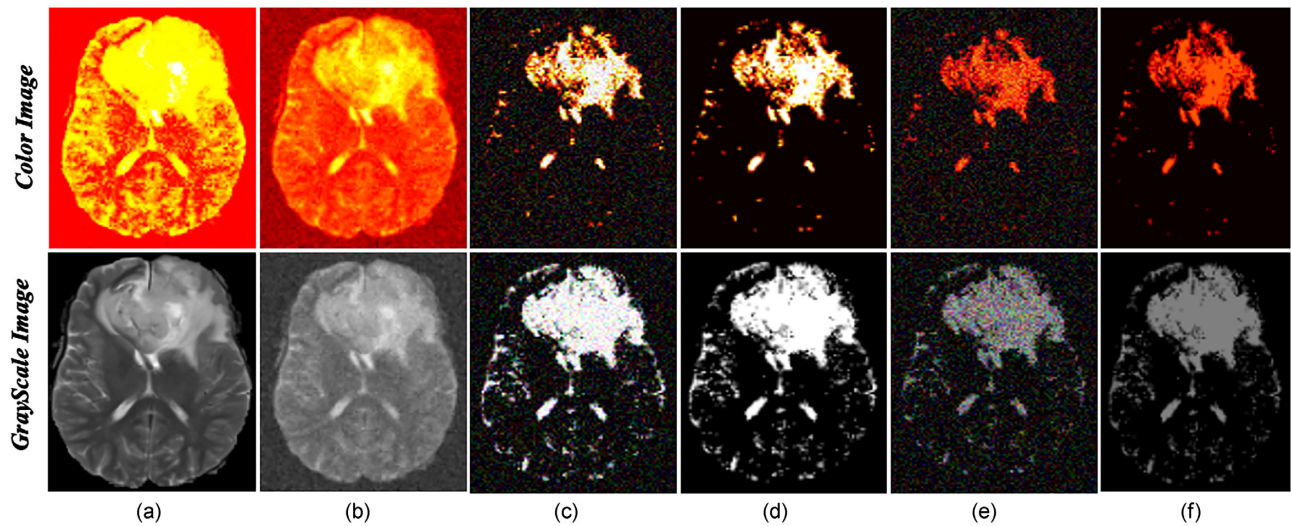


**Figure 9:** MRF segmentation of a brain tumor. From left: (a) An MR image T2 modality of a human brain tumor, (b) noisy image, (c) naive Bayes image with noisy, (d) naive Bayes image without noisy, (e) MRF image with noisy, and (f) MRF image without noisy.

Because of the complexity and diversity of the anatomic models in tumor structures, it is difficult to segment structures from medical images and reconstruct a geometric representation of these structures.

Deformable models are curves in 2D or surfaces in 3D formed inside an image domain that may move according to a speed function controlled by global and local forces (Gordillo et al., 2013). The model local and global attributes are determined so as to conform to an object boundary or other desirable features within an image.

Surface-based segmentation methods can be used to segment regions with boundary deficiencies like missing edges and lack of texture contrast between the background and ROIs (Saman & Jamjala Narayanan, 2019). Deformable models can be divided as parametric active contour models (ACM) and geometric deformable models as follows:

### 3.3.2.1. Parametric active contour models

Active contour models (or snakes) have been extensively used in many brain tumor segmentation applications, where it has the capability of accommodating the usually considerable variability of biological structures and the ability to segment and track anatomic structures in MRI images by exploiting restrictions derived from the image data in conjunction with a priori knowledge about the size, location, and structures shape (Gordillo et al., 2013).

Active contours are simply connected closed curves that work to define smooth shape in the image and trace the boundary via corresponding the deformable model with the image curve, affected by weighting attributes (global and local forces) in order to reduce the specific energy function (Wadhwa et al., 2019) that controls the elasticity and solidity of the curve (Rajendran & Dhanasekaran, 2012).

The global forces push the curve to move toward the desired boundaries, while the local forces work to assure the softness of the model during the deformation process. In order to not find the local minima away from the contour, the snake must be initialized near the intended contour as shown in Fig. 10.

Deformable active contour model is a curve  $X(i) = [x_i, y_i]$ ,  $i = [0, \dots, n]$ , that moved to connect collection of  $n$  points within the image to reduce the energy function, where the global energy of active contour function is zero at the edges, and only positive in

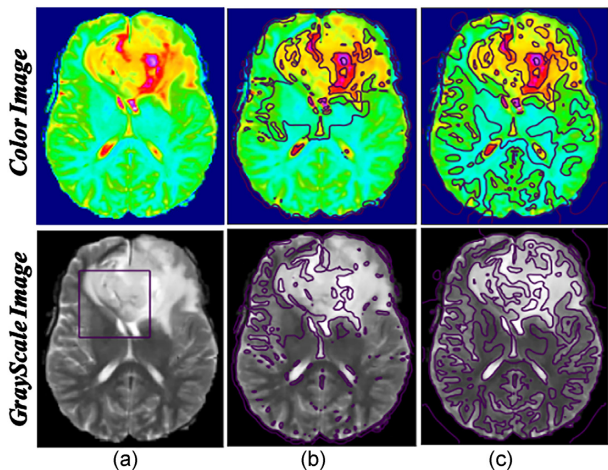


**Figure 10:** Segmentation of brain MRI image (T2 modality) using active contour.

homogeneous regions (Chan & Vese, 2001). For gray-level images, active contours did not perform well due to the presence of sharp corners and concavities, which was overcome by presenting the gradient vector flow (GVF) proposed by Xu and Prince (1997, 1998). However, GVF needs prior knowledge of objects and adequate parameter selection for good and consistent results. Furthermore, it requires complex computations.

Active contour deformation models are characterized by its sensitivity in the search for boundaries of brain tumors, where the sensitivity of the boundaries discovered by the active contours is better than traditional edge detection approaches.

### 3.3.2.2. Geometric deformable models or level sets

Due to the difficulty in dealing with the topological changes of dividing and merging of contours when using parametric deformable models for volumetric 3D image segmentation, geometric deformable models have been developed to solve this problem based on curve evolution theory and level set (Malladi et al., 1995; Safavian et al., 2020; Xu et al., 2000b). Although these approaches have been notably successful in initializing the active parametric

contours, it is difficult to achieve this in tumor segmentation of MRI images because many segmentation approaches cannot deal with regularly shaped objects (Kichenassamy et al., 1995; Liu et al., 2014). In addition, images are noisy with edges that are not clearly defined, which may result in topologies incompatible with the actual object (Xu et al., 2000a).

Geometric deformable models are most commonly used for MRI image segmentation and finding single objects within an image. Although several approaches have been proposed for MRI image segmentation using deformable models, their utility is severely limited.

Ho et al. (2002) developed a method for automatically segmenting the anatomical structures of tumor in 3D MRI images. To guide a level set snake propagation, the segmentation was done using a map to determine the probability for tumor regions and background. The proposed method prevents the snakes from leaking through weak or missing border parts by modulating the propagation term with a signed local statistical force, leading to a stable solution.

Li et al. (2008) proposed a region-based active contour model that draws upon intensity information in local regions in a variational level set formulation for the segmentation of brain MRI. They determined a data suitable energy in terms of a contour, in addition, two suitable functions that locally approximate intensities of the image on both sides of the contour. After incorporating this energy into a variational level set formulation with a regularization term, a curve evolution equation for energy minimization is derived.

Bogovic et al. (2013) proposed a multiple object segmentation method based on a geometric deformable model that ensures object relationships and topology, eliminates gaps or overlaps, allows for boundary-specific speeds, and offers a computationally efficient growth scheme that is independent of objects number.

### 3.4. Hybrid techniques

The idea of hybrid techniques is based on combining two or more techniques in order to benefit from their advantages to get better segmentation and fruitful and reliable results. This combination may produce better segmentation accuracy, especially for brain MRI segmentation applications (Li et al., 2011; Xue et al., 2003).

Parveen and Singh (2015) proposed a hybrid technique that combined SVM and FCM to obtain an accurate classification of the tumor region in the brain. Initially, the image contrast was improved using enhancement techniques, and the skull was stripped using dual-threshold and morphological operations. FCM clustering was utilized for image segmentation to detect suspect regions in brain MRI images. To extract the features from the MRI image, the gray level run length matrix is used, and after that, the SVM technique is used to classify the brain MRI images, which gives more accurate and efficient results for brain MRI image classification.

Akselrod-Ballin et al. (2006) presented hybrid technique by integrating SVM-based classification to identify the brain structures in MRI and multi-scale segmentation weighted aggregation. The segmentation yields a complete hierarchy, which is represented as an irregular pyramid. The pyramid represents the image in a rich, adaptable manner, allowing detection of different anatomical structures at various scales. Nyma et al. (2012) proposed a hybrid technique for MRI image segmentation that combines Otsu thresholding with FCM. As an initial coarse segmentation approach, Otsu thresholding was used to detect the homogenous regions of the input image, then FCM was employed to segment

brain MR images into several segments. Vaibhavi and Rupal (2018) suggested a hybrid technique combining the k-means and FCM algorithms for brain tumor segmentation in MRI images and compared the results with the individual results of the FCM and k-means algorithms.

Hamad et al. (2019) proposed a hybrid technique combination of FCM and threshold approach to detect brain tumor in MRI images. The proposed method focuses on a noise elimination technique, and image contrast enhanced using a balance contrast enhancement technique. The FCM was used to segment the normal brain region and threshold approach to convert the enhanced image to binary image to segment the tumor region in MRI images. Then, to detect the fine edges, the Canny edge detection method was used.

Zhang et al. (2019a) proposed a hybrid clustering technique combining k-means++ and FCM algorithms with morphological operations for brain tumor segmentation. Morphological operations were used to remove non-brain tissue from the MR brain image, thus effectively reducing the sensitivity of noise. The k-means++ was employed for deterministic initialization of cluster centroids to avoid overfitting, and the Gaussian kernel-based FCM was used to perform clustering, which further improved the ability of classification.

## 3.5. Deep learning techniques

In recent years, image segmentation has become a common task in medical image analysis and has been powered by deep learning techniques. Currently, brain tumor segmentation using deep learning techniques based on CNNs is one of the researchers' interests in order to obtain accurate segmentation methods that enhance the task of determining tumor regions. Recently, several CNN-based approaches have been proposed for brain tumor segmentation (Table 1 illustrates some of the models used for brain tumor segmentation). In this subsection, architectural details of some recent CNN-based models of segmentation are presented on the basis of the most important feature used in each architecture.

### 3.5.1. Based on fully convolutional network approach

The idea of a fully convolutional network (FCN) was presented by Long et al. (2015), where they transfer the classifiers layer in the basic CNNs (Simonyan & Zisserman, 2015; Szegedy et al., 2015) to dense FCN layers by replacing fully connected layers (dense layers) with  $1 \times 1$  convolutional layers. FCN attempts to learn representations based on only local information, whereas it loses the global semantic context of the image, which makes segmentation quite ambiguous. Therefore, the basic model VGG-16 helped the FCN model to achieve effective results by skipping connections for merging low-layer and high-layer features in the final layer for segmentation.

Sun et al. (2021) proposed a multi-pathway 3D architecture based on a FCN for glioma segmentation in MRI images. The architecture employs 3D dilated convolution in each pathway to extract different receptive fields of feature maps from multi-modal MRI images, which are then spatially fused using skip connections. This architecture can help FCN models better pinpoint tumor region boundaries.

### 3.5.2. Based on cascaded CNN approach

The cascaded architecture is used as a choice for joint segmentation models, which are usually more computationally expensive. The idea of a cascaded architecture is based on a sequence of connected CNNs architecture where the output of one CNN becomes

**Table 1.** Summary of some recent deep learning methods based on brain tumor segmentation with regard to the different BraTS datasets, MRI modalities, model architecture, optimization (initial learning rate), activation function, and dice coefficient (DSC). Note: ET – Enhancing tumor; WT – Whole tumor; TC – Tumor core; and NA – Not available.

Name	Dataset	MRI modality	Model architecture	Optimization algorithm	Activation function	DSC		
						WT	TC	ET
Sun et al. (2021)	BraTS 2019	T1, T1c, T2, and FLAIR	3D FCN	Adam(0.002)	RReLU	0.89	0.78	0.76
	BraTS 2018	T1, T1c, T2, and FLAIR						
Havaei et al. (2017)	BraTS 2013	T1, T1c, T2, and FLAIR	Cascaded CNN	SGD, Momentum ( $\mu = 0.05, \sigma = 0.005$ )	Maxout	0.88	0.79	0.73
Hussain et al. (2017)	BraTS 2013	T1, T1c, T2, and FLAIR	Cascaded DCNN	Momentum ( $\mu = 0.05, \sigma = 0.003$ )	ReLU	0.80	0.67	0.85
Pereira et al. (2017)	BraTS 2013	T1, T1c, T2, and FLAIR	Hierarchical FCN	SGD(0.01)	LReLU	0.85±0.05	0.76±0.17	0.74±0.08
Ranjbarzadeh et al. (2021)	BraTS 2013	T1, T1c, T2, and FLAIR	Cascade CNN model and distance-wise attention	Adam( $10^{-4}$ )	ReLU	0.92	0.87	0.91
Wang et al. (2017a)	BraTS 2017	T1, T1c, T2, and FLAIR	Cascaded FCN	Adam( $1 \times 10^{-3}$ )	PReLU	0.90	0.83	0.78
Wang et al. (2019a)	BraTS 2018	T1, T1c, T2, and FLAIR	Cascaded CNN	Adam( $1 \times 10^{-3}$ )	PReLU	0.90	0.85	0.79
Jiang et al. (2020)	BraTS 2019	T1, T1c, T2, and FLAIR	Cascaded U-Net	Adam( $1 \times 10^{-4}$ )	ReLU	0.88	0.83	0.83
Chen et al. (2019)	BraTS 2018	T1, T1c, T2, and FLAIR	3D dilated multi-fiber network (DMFNet)	Adam(0.001)	ReLU	0.90	0.84	0.80
Wang et al. (2021)	BraTS 2019	T1, T1c, T2, and FLAIR	Dilated feature pyramid based on residual module and U-Net (DFP-ResUNet)	Adam( $1 \times 10^{-4}$ )	ReLU, LeakyReLU	0.90	0.84	0.79
Kamnitsas et al. (2018)	BraTS 2017	T1, T1c, T2, and FLAIR	Ensembles of multiple models based on FCN and U-Net	Adam, AdaDelta	ReLU	0.88	0.78	0.72
Cahall et al. (2021)	BraTS 2018	T1, T1c, T2, and FLAIR	Dilated inception U-Net (DIU-Net)	Adam( $10^{-4}$ )	ReLU	WT = 0.925±0.931 and TC = 0.952±0.957		
Yang et al. (2020)	BraTS 2018	T1, T1c, T2, and FLAIR	Dilated convolution U-Net (DCU-Net)	NA	ReLU	0.91	0.78	0.83
Zhang et al. (2021)	BraTS 2020	T1, T1c, T2, and FLAIR	Multi-encoder net (ME-Net)	NA	ReLU	0.88	0.73	0.70
Guan et al. (2022)	BraTS 2020	T1, T1c, T2, and FLAIR	Encoder-decoder (AGSE-VNet)	NA	ReLU	0.85	0.69	0.68
Baid et al. (2020)	BraTS 2018	T1, T1c, T2, and FLAIR	3D U-Net architecture	Momentum ( $\alpha = 0.001$ )	ReLU	0.85	0.77	0.67
Ali et al. (2020)	BraTS 2019	T1, T1c, T2, and FLAIR	3D CNN and 3D U-Net architecture	Adam( $3 \times 10^{-4}$ and $1 \times 10^{-3}$ )	LReLU	0.90	0.84	0.75
Rehman et al. (2021)	BraTS 2017	T1, T1c, T2, and FLAIR	Encoder-decoder (BrainSeg-Net) architecture	Adam	ReLU	0.89	0.79	0.74
	BraTS 2018							
Rehman et al. (2020)	BraTS 2018	T1, T1c, T2, and FLAIR	BU-Net architecture based on encoder-decoder	Adam(0.01)	ReLU	0.90	0.83	0.78
Kamnitsas et al. (2017a)	BraTS 2015,2016	T1, T1c, T2, and FLAIR	DeepMedic	NA	NA	0.89	0.75	0.71
Wang et al. (2019b)	BraTS 2018	T1, T1c, T2, and FLAIR	Cascade nested dilation networks with SE blocks and RnD blocks	Adam(0.0001)	ReLU	Edema(0.70) non-EN(0.58) EN(0.72)		
Jiang et al. (2022)	BraTS 2018,2019	T1, T1c, T2, and FLAIR	Multi-resolution fusion network based on inception U-Net (MRF-IUNet)	Adam	NA	0.83	0.93	0.94
Li et al. (2019)	BraTS 2015,2017	T1, T1c, T2, and FLAIR	Inception-based U-Net and modified cascade and up skip connection	Adam(0.01)	ReLU	0.87	0.76	0.64
Zhou et al. (2020)	BraTS 2013,2015,2018	T1, T1c, T2, and FLAIR	Dense connectivity with atrous convolutional feature pyramid (DCNNs)	RMSprop(0.001)	ReLU	0.86	0.77	0.75
Huang et al. (2021)	BraTS 2018	T1, T1c, T2, and FLAIR	A multi-depth fusion module based on V-Net structure	Adam(0.0001)	ReLU	0.80	0.75	0.71
	BraTS 2019							
Zhou et al. (2021)	BraTS 2020	T1, T1c, T2, and FLAIR	Encoder based on ShuffleNetV2 and shallow decoder based on residual (ERV-Net)	Adam(0.0003)	LReLU( $\sigma = 0.01$ )	0.91	0.86	0.81
Karayegen & Aksahin (2021)	BraTS (NA)	T1, T1c, T2, and FLAIR	Down-sampling and up-sampling architecture	NA	ReLU	Accuracy (0.957) and F-score (0.93)		
Ben naceur et al. (2020)	BraTS 2018	T1, T1c, T2, and FLAIR	DCNN (sparse-multi-OCM and dense-multi-OCM)	Adam, SGD(0.001)	ReLU	0.90	0.83	0.83

**Table 2.** The strengths and limitations of the most used segmentation methods for brain tumor MR images.

Methods	Strengths	Limitations
<b>Conventional-based segmentation methods</b> Thresholding (global and local) (Aranguren et al., 2021; Tarkhaneh & Shen, 2019)	Simple execution with fast computation time.  Important for any type of segmentation and useful for image linear.	These techniques are ineffective for all types of brain MRI images due to the high-intensity variance in image intensity. Limited applicability to improving different tumor regions, and lower performance in heterogeneous regions. Affected by noise and require user intervention. May produce oversegmentation or holes due to noise or difference in intensity, and requires a post-processing step. The problem with the watershed is its sensitivity to intensity variations when the image is segmented into several large regions. Oversegmentation.
Region growing (Al-Faris et al., 2014; Salman et al., 2005b)  Watershed (Kuo et al., 2008; Preim & Botha, 2014)	Simple and capable of separating the regions that have similar attributes and high performance in the complicated regions. The perfect technique for grouping similar pixels in an image based on their intensity.  Divides multiple regions at the same time.	Collecting training samples is difficult, and the learning phases are generally slow. It requires more time for training and is computationally intensive.
<b>Supervised-based segmentation methods</b> Artificial neural network (ANN; Tripathi et al., 2018; Wang et al., 2015) Random forest (RF; Goetz et al., 2016; Soltaninejad et al., 2018b)	ANN is highly dependent on complex and multi-variate non-linear domains. RF is flexible in a classification problem and uses a rule-based technique. Helps to improve decision tree accuracy by reducing overfitting. k-NN is easy to understand, very time-efficient, and easy to implement as the only thing that needs to be calculated is the distance between different points.	Since all the work is done at run-time, k-NN can have poor performance with a large dataset, and the computation would be very expensive. Sensitive to noise, and the value k affects the performance of the algorithm. Not suitable for large datasets because it takes a long time to train. Not suitable when the dataset has more noise. The standard convolution operation used on conventional grids is inefficient when applied to superpixels.
K-nearest neighbor (k-NN; Cunningham & Delany, 2020; Ramteke & Monali, 2012)		
Support vector machine (SVM; Sathies Kumar et al., 2017; Suthaharan, 2016)		
Superpixel-based segmentation (Alipour & Hasanzadeh, 2021; Imtiaz et al., 2020; Soltaninejad et al., 2017)		
<b>Unsupervised-based segmentation methods</b> Markov random fields (MRFs; Ahmadvand et al., 2017; Yousefi et al., 2012)	An efficient approach to minimize the number of image primitives subsequently required for further processing.	
k-Means clustering (Saman & Jamjala Narayanan, 2019; Wadhwa et al., 2019)	The spatial information is preserved within the contextual restrictions of neighboring pixels.	It is only effective in tissues that are homogeneous, and is therefore not commonly used in heterogeneous tissue classes. Difficulty in determining the factors that govern the intensity of spatial interactions. It needs computationally expensive. It can produce poor and imprecise results in the case of an improper selection of value k.
Fuzzy c-means (FCM) clustering (Ganesh et al., 2017; Setyawan et al., 2018)	It may describe complicated relationships between data instances. More effective against noise. Efficient and simple clustering technique that works fast enough for real-time image segmentation. Less complex technique. Determines the degree of membership of the data for each category. It can converge the boundaries of tumor.	Long computational time, sensitive to noise and outliers. Sensitivity in centroid initialization, therefore different initializations lead to different results. It uses the non-robust Euclidean distance. Not entirely appropriate for situations where regions do not have clearly specified boundaries. Relatively slow and sensitive to noise. Active contours based on edges may ignore blurred boundaries. Computationally costly.
Parametric active contours (Gordillo et al., 2013; Wadhwa et al., 2019)	It allows soft clustering. Ensure accurate computation and eliminate costly recurring initialization procedures. Adaptable to the variability of biological structures.	
Level set (Bogovic et al., 2013; Safavian et al., 2020; Virupakshappa & Amarapur, 2019)	Able to naturally deal with topological changes and 3D effects. Extracting complex shapes.	It requires manually calculating parameter values at each level. Time-consuming and boring to apply to different brain images. It requires a high and sophisticated computational effort. It depends on the combination of feature selections from different methods.
<b>Hybrid techniques</b> (Hamad et al., 2019; Parveen & Singh, 2015; Zhang et al., 2019a)	Hybrid techniques are aimed at combining the benefits of many models into a single approach. More adaptable and flexible when dealing with high-dimensional data. Hybrid techniques integrate the relative strengths of several classifiers and use them in such a way as to enhance the overall accuracy. Since deep learning algorithms are good at learning on their own, it is no longer required to use well-labeled data. It works to encode spatial information to obtain further structured results.	It requires high computational time, large amounts of storage, more effective GPUs, and a lot of resources.
<b>Deep learning techniques</b> (Chen et al., 2020; Guan et al., 2022; Li et al., 2019; Pereira et al., 2016; Zhang et al., 2020)	High performance for intra-tumor segmentation.  In deep learning techniques, problems are often solved on an end-to-end basis, whereas traditional methods are not able to do so.	Unreliable for real-time applications and often requires a post-processing step.  Data labeling can be an expensive and time-consuming operation.

a direct input to different levels of the other CNNs (Havaei et al., 2017; Hussain et al., 2017). This improves-on approaches that perform multi-scale predictions separately, like dual-path methods, where contextual information is connected to the other CNNs as additional image channels through the input cascade.

In a cascaded architecture that depends on the concatenation of local pathways (Havaei et al., 2017), the output of the first CNNs is connected with the first hidden layer output of the second CNNs. Another form of cascading architecture is hierarchical sub-regions segmentation concatenation (Pereira et al., 2017; Wang et al., 2017a, 2019a). In this architecture, brain tumor subregions are sequentially segmented by decomposing the multiple-class segmentation problem into multiple stages of binary segmentation tasks. Therefore, this architecture exploits the hierarchical nature of brain tumor subregions to reduce the number of false positives and lessen the effects of class imbalance problems.

Wang et al. (2017a) proposed three hierarchical networks sequentially to segment subregions of brain tumors. The first network (WNet) separates the whole tumor from the MRI images multi-modal in order to obtain the bounding box of the whole tumor, which is then used as the input to the second network (TNet) to segment the tumor core. The output of the second network is the bounding box of the tumor core, which is fed into the third network (ENet) to segment the enhancing tumor. This work is expanded in Wang et al. (2019a), which exploits test-time augmentation to acquire uncertainty estimates of segmentation results as well as a CRF for post-processing. Moreover, more ablation trials are conducted to verify the efficacy of pipeline segmentation.

Jiang et al. (2020) proposed a two-stage cascaded network to segment the substructures of brain tumors from coarse to fine. In the first stage, a variation of U-Net was employed to train a coarse prediction. In the second stage, two decoders are used to improve performance by widening the network. This improves the prediction map by concatenating the original input with a preliminary prediction map to use auto-context.

### 3.5.3. Based on dilated/atrous convolution approach

The dilated convolution (also called atrous convolution) approach is a modified version of the classic CNNs presented by Yu and Koltun (2015) in order to systematically collect multi-scale contextual information to improve segmentation without suffering resolution loss. In contrast to conventional pyramidal CNNs, the dilated approach allows exponential growth of receptive fields and linear parameter accretion without losing spatial information, which is able to produce more effective features from input data than the standard convolution with the same parameter. The benefit of a dilated-based model is that it preserves the spatial resolution of the image in order to provide a dense forecast. However, the employment of dilated convolution separates image pixels from its global context, making it susceptible to misclassification.

Chen et al. (2019) proposed a greatly efficient 3D DMFNet that used the multi-fiber (MF) and dilated multi-fiber (DMF) units as the building blocks to achieve dense volumetric segmentation in real-time. The network leverages the 3D DMF unit inspired upon the MF unit (Chen et al., 2018), which consists of an ensemble of lightweight 3D convolutional networks to greatly reduce the computational cost while maintaining high accuracy for brain tumor segmentation. The key components of the DMF unit are as follows: (i) “channel grouping”, the idea of channel grouping depends mainly on reducing the connections between feature maps and the kernels to provide parameters significantly by splitting the convolutional channels as multiple groups; (ii) “multi-plexer” to

facilitate the exchange of information between fibers; and (iii) “dilated fiber” to magnify the respective field and capture multi-scale 3D spatial correlations of brain tumor lesions.

Cahall et al. (2021) proposed the DIU-Net architecture for end-to-end brain tumor segmentation based on U-Net, which combines inception modules and dilated convolutions in both contracting and expanding pathways to extract both local structural and global contextual information. In this architecture, each dilated inception module comprises three  $1 \times 1$  convolution operations followed by an  $l$ -dilated convolutional filter, where  $l = 1, 2$ , and 3.

Another study by Yang et al. (2020) proposed a novel architecture (DCU-Net) with dilated convolution for brain tumor segmentation based on the traditional U-Net. The field of feature reception can be expanded while keeping image resolution by replacing max pooling at the end of the down-sampling pathway with dilated spatial pyramid pooling. In order to improve the network ability to identify tumor features more accurately, both skip connections and dilated convolution residual blocks are combined in the training networks.

### 3.5.4. Based on the top-down/bottom-up approach

This type of architecture consists of down-sampling and up-sampling stages, also known as the encoder and decoder stages, respectively. The idea of this type is to create two paths for segmentation. The first path works to extract features from images and reduces the image dimension by a series of convolutional and pooling layers (another way to get the reduction effect is too convolutional with increasing step length instead of the pooling layer) to obtain low-resolution feature maps. The second path works in reverse of the first path, which increases the size of the image dimensions by deconvolution layers (also called fractionally strided convolutional or convolutional transpose) to generate the desired class's localization. In certain cases, the sequence is incorporated between intermediate feature maps or unpooling layers (Zeiler & Fergus, 2014) to improve the resolution of the final result.

So far, many important architecture have been proposed for general medical segmentation based on a top-down/bottom-up approach, such as the U-Net architecture (Ronneberger et al., 2015) and the V-Net architecture (Milletari et al., 2016). This architecture was used afterward for brain tumor segmentation in different hierarchy from one architecture to the next depending on the proposed approach. To improve the V-Net architecture, which has only one down-sampling path, Zhang et al. (2021) proposed an architecture called a ME-Net comprised of four similar encoder structures to enable segmentation of the MRI modalities images, eventually merged into feature maps and fed to the decoder structure by skipping connections. In addition, the feature maps of the corresponding down-sampling stage are merged into the up-sampling operation to make up for any information that was lost.

Guan et al. (2022) proposed an automatic framework called 3D AGSE-VNet for brain tumor segmentation using 3D MRI images, which is an end-to-end network combined segmentation architecture based on V-net using an integrated module of the squeeze and excites (SE) for each encoder and the attention guide filter (AG) for each decoder, improving the useful information automatically using the channel relationship. The performance of this model was tested on the brain tumor segmentation challenge (BraTS) 2020 dataset and achieved effective segmentation results and has the possibility of clinical experiments.

Baid et al. (2020) proposed a 3D fully automated brain tumor segmentation architecture based on the U-Net model that partitions radiologically identifiable tumor subregions and

addresses the class imbalance problem between non-tumor and tumor spots through the process of extracting a weighted patch from the border regions of the tumor. The results showed that when there is a slim border between tumor subparts, the weighted patch-based segmentation method gives similar performance to the pixel-based method.

Ali et al. (2020) suggested a segmentation architecture 3D CNNs alongside a U-Net architecture, in a combinative technique that results in better segmentation and accurate predictions. The first architecture used 3D CNNs initially developed by Chen et al. (2019); this architecture used MF blocks with adaptive weighted dilated convolutions to glean feature representation at multi-scale for volumetric segmentation and allowing flowing and capturing spatial information. The second architecture is a 3D U-Net which is various from the traditional U-Net architecture, that the hyperparameters used in this architecture have been replaced. The network showed good results in the BraTS 2018 challenge compared to other networks.

Pereira et al. (2016) proposed an automatic segmentation method based on CNN for a deeper architecture design. The architecture has been segmented into special cases for HGG and LGG, to reduce the complexity of large variability in intra-tumoral structures. The proposed architecture used for HGG cases is deeper than the one of LGG cases because going deeper did not improve results in LGG cases.

HGG CNNs architecture includes 11 layers, six convolutional with filter size  $3 \times 3$  and stride  $1 \times 1$ , two max-pooling with filter size  $3 \times 3$ , stride  $2 \times 2$ , and three fully connected layers, while the architecture of LGG CNNs includes nine layers, four convolutional with filter size  $3 \times 3$  and stride  $1 \times 1$ , two max-pooling with filter size  $3 \times 3$ , stride  $2 \times 2$ , and three fully connected layers.

Rehman et al. (2020) have proposed an encoder-decoder-based model named BU-net to contribute to brain tumor segmentation research, this architecture is characterized by the use of residual extended skip and wide context in the U-Net architecture. These modifications produce more diverse features, by increasing the valid receptive field, wherein in previous basic architecture, no contextual information is shared between the shallow and deep layers. Also, Rehman et al. (2021) have proposed an encoder-decoder-based model named BrainSeg-Net to address the problem of getting lost spatial details along with location information due to non-linear transformations and continuous convolutions in deeper layers. BrainSeg-Net used a feature enhancer (FE) block which extracts medium-level features from low-level features from the shallow layers and shares them with the dense layers and reproduces spatial and location information during the up-sampling process. BrainSeg-Net architecture contains an encoder and decoder path, the encoder and decoder include four blocks, in addition to a single transition at bottom of the architecture, every encoder block and its associated decoder block connected to the FE block. The output of the FE block is concatenated with the output of all the deeper stage FE blocks, then the output is concatenated with the output of the corresponding transformation layer from the decoder block. The FE block improves segmentation performance and helps identifying small regions of the tumor. Furthermore, the skip connection of the FE block allows recovering the fine details that were lost during the down-sampling process. BrainSeg-Net architecture achieved good segmentation results by three benchmark datasets, namely BraTS2017, BraTS2018, and BraTS2019.

Kamnitsas et al. (2017a) proposed architecture DeepMedic which consisted of 11-layer 3D CNNs with residual connections. The architecture consists of two parallel convolutional pathways,

each of which processed the input at a specific scale to give a large reception field for the final classification while maintaining the computational cost minimal.

Casamitjana et al. (2017) proposed two fully convolutional 3D CNNs architecture, and also trained another model that represents the two-pathway DeepMedic net proposed by Kamnitsas et al. (2017b). The first model, 3DNet\_1, is a 3D FCN based on the VGG architecture (Simonyan & Zisserman, 2015), with skip connections that combine high- and low-layer information. The second model, 3DNet\_2, is the 3D version of the network proposed in Ronneberger et al. (2015). The third architecture, 3DNet\_3, is a modification of DeepMedic network (Kamnitsas et al., 2017b). The objective of using two paths is to collect both high- and low-resolution features from the input segment while using various input sizes for each path. All models use the Rectified Linear Unit (ReLU) activation function, batch normalization, and Adam optimization for training. All models achieved remarkable segmentation accuracies. Three models were trained and tested on BraTS 2015 training dataset (60% of the data for training and the remaining 40% for testing).

In MRI brain tumor segmentation, the interest in deep learning is mostly initiated by CNNs. According to CNNs, it is an effective way to learn representations and extract features from images. The building blocks of CNNs are different based on the type of segmentation (semantic segmentation, instance segmentation, and panoptic segmentation) according to Sultana et al. (2020). In this subsection, we focus on the building blocks of CNNs-based semantic segmentation and evolution based on the top-down and bottom-up approaches (encoder-decoder path).

## 4. CNN for Image Segmentation

In deep learning, a CNN is one of deep neural networks algorithms and, most commonly, which have outperformed the state-of-the-art in many visual recognition tasks. A CNN typically includes a sequence of computation layers stacked together (Zhao et al., 2017). These layers learn input feature maps and produce output feature maps. The first layer in image segmentation is an input image, and the last layer is an output image with class labels assigned to each pixel. In CNN-based segmentation algorithms, predominantly the segmentation results are achieved by “upsampling” the input image using deconvolution layers in CNNs.

Recently, research has shown that use of CNNs in the segmentation of brain tumor can be a very promising approach (Havaei et al., 2017; Seo et al., 2021; Zikic et al., 2014). Some recent works have focused on medical tasks, and several of them include designs that are well suited to medical images or brain tumor segmentation in particular (Chen et al., 2017; Guo et al., 2015; Havaei et al., 2017; Kamnitsas et al., 2015; Karthik et al., 2019; Maier et al., 2015).

The idea behind CNNs is to identify and detect features. Therefore, we need to comprehend the basic building blocks of CNNs used for image segmentation. In this survey, we selected the most common method for segmenting MRI images in recent years, as shown in Fig. 12, which consists of two paths, as follows:

### 4.1. Encoder network path

The encoder path is mostly based on the VGG-16 network (Simonyan & Zisserman, 2015) except FC layers, and most CNNs used for segmentation are very similar to this path. In summary, the encoder path reduces the dimension of the image by half in every pooling layer. During the encoder, the feature information

is increased while spatial information is decreased (Ronneberger et al., 2015). The significance behind this path is to interpret the image context related to what kind of information is current in the image (Karthik et al., 2019). In this path, we discuss the main layers such as convolutional, non-linearity, and pooling/dilation convolution layers.

---

**Algorithm 1:** A convolutional neural networks (CNN) encoder path: Training starts with  $H_1 \times W_1 \times N_C$ . Additional parameters required in training are  $H_1$  height of the input feature map,  $W_1$  width of the input feature map,  $N_F$  number of filters,  $N_C$  number of channels,  $N_L$  number of layers,  $P$  zero padding and  $S$  stride rate.

---

```

Input: A feature map  $I$  of shape  $H_1 \times W_1 \times N_C$ .
Input: A coefficient matrix  $K$  of shape  $N_F \times H_1 \times W_1 \times N_C$ 
Output: A feature map  $O$  of shape  $H_2 \times W_2 \times N_C$ 

Encoder CNN:
1 input  $H_1 \times W_1 \times N_C$ 
2 for  $L \leftarrow 0$  to  $N_L - 1$  do
3   for  $f \leftarrow 0$  to  $N_F$  do
4     for  $c \leftarrow 0$  to  $N_C$  do
5        $O_{Lf} \leftarrow O_{Lf} + \text{conv}(I[c], K[f, c])$ 
6     end
7   end
8    $Pool_L, Pool_k \leftarrow \text{pool}(O_{Lf})$ 
9   if  $L \leq N_L$  then
10     $O_{Lf} \leftarrow Pool_L$ 
11  else
12    return  $Pool_L, Pool_k$ 
13  end
14 end

```

---

#### 4.1.1. Convolutional layers

The convolutional layer is one of the major building blocks of the encoder path of any CNN-based segmentation, which does the majority of the computation. The convolutional layer is the simple application of a filter to an input image with the convolution kernel, producing one output feature map. There are often groups of several convolution kernels used in one layer and thus multiple filters of output feature maps are produced. Repeated application of the same filter to an input results in a map of activation called a feature map, indicating the locations and strength of a detected feature in an input.

A convolutional layer includes a collection of filters whose parameters need to be learned. The height and weight of the filters must be smaller than the input size, as well as each filter is combined with the input size to compute an activation map made of neurons (Ke et al., 2018).

Convolutional layers help to learn the relationships between the pixels of input images by extracting representative features. The features detected in each layer vary based on its complexity, with the first layer extracting simple features, such as edges, while the subsequent layers extract more complex and high-level features (Bernal et al., 2018).

In the convolutional layer, a collection of filters with small parameters is used, often  $3 \times 3$  in size, as Fig. 11, the convolution layer can be described as follows:

$$O_L = \sum_{f=1}^{N_f} \sum_{c=1}^{N_C} \text{conv}(I[c], K[f, c]). \quad (9)$$

This equation means that each output filter will sum up all convolution results between each channel of the input feature map ( $I[c]$ ) and the kernel ( $K[f, c]$ ). Given  $f$  is the filter index,  $N_f$  is the total

number of filters,  $c$  is the channel index, and  $N_C$  is the total number of channels.

---

**Algorithm 2:** A convolutional neural networks (CNN) decoder path: input pooling mask and pooling indices having a size of  $H_2 \times W_2 \times N_C$  from encoder network. It requires hyperparameters,  $N_F$  number of filters,  $N_C$  number of channels,  $N_L$  number of layers,  $H_O$  height of the output feature map,  $W_O$  width of the output feature map,  $N_O$  number channels of the output feature map,  $P$  amount of zero padding and  $S$  stride rate.

---

```

Input: A feature map  $I$  of shape  $H_2 \times W_2 \times N_C$ .
Input: A coefficient matrix  $K$  of shape  $N_F \times H_2 \times W_2 \times N_C$ 
Output: output feature map of shape  $H_O \times W_O \times N_O$ .

Decoder CNN:
De-Conv and upsampling / unpooling:
1 input  $Pool_L, Pool_k$ 
2 for  $L \leftarrow N_L - 1$  to  $1$  do
3   if  $L \geq 1$  then
4      $O_L \leftarrow \text{Upsample}(Pool_L, Pool_K)$  // or Unpooling or
      deconv
5   else
6     return  $O_{Lf}$ 
7   end
8   for  $f \leftarrow N_F$  to  $0$  do
9     for  $c \leftarrow N_C$  to  $0$  do
10     $O_{Lf} \leftarrow O_{Lf} + \text{conv}(I[c], K[f, c])$ 
11  end
12 end
13  $Pool_L \leftarrow O_{Lf}$ 
14 end
15 return  $O_{Lf}$ 

```

---

#### 4.1.2. Non-linearity layers

In any neural network, the activation functions play a major role in determining the final performance of the trained network, and they help to learn and make sense of non-linear and complex mappings between inputs and corresponding outputs (Sharma et al., 2020). A non-linear transformation is performed on the feature maps generated by the convolutional layer and passed to the pooling layer to further modify the output (Sonoda & Murata, 2017). Non-linear transformations can be acquired using a specialized class of functions known as activation functions that make the network able to learn sparse non-trivial representations. As a result, the network becomes more dynamic, able to extract complicated features from data, and more tolerant to slight noise or modifications in the input data. Moreover, the computational efficiency of representations is boosting.

The most common and simple activation function is the ReLU, which is defined as  $f(x) = \max(0, x)$ , where ReLU commonly does not suffer from vanishing or bursting gradients and learns faster (Agarap, 2018). However, the disadvantage of ReLU is the saturation of the network with a constant zero gradient, which causes the network to converge slowly. To solve the problem of constant zero-saturation, Maas et al. (2013) proposed leaky ReLU (LReLU) allows slight non-zero gradient flow when the network is saturated. This function is represented as  $f(x) = \max(x, 0) + \sigma \min(0, x)$ , where  $\sigma$  is a constant parameter of leakiness (commonly 0.01). For more information about another common activation function see He et al. (2015) and Clevert et al. (2015).

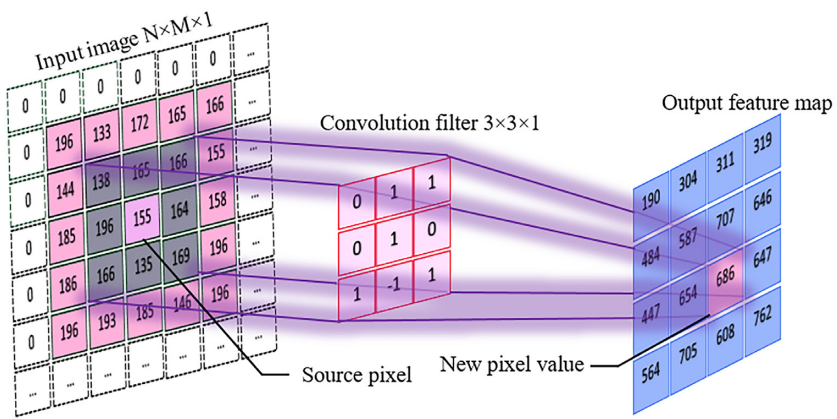


**Figure 11:** A filter applied to a 2D input to create a feature map. When the filter is applied multiple times to the input array, the result is a 2D array of output values that represent the input filter. As such, the 2D output array of this operation is called a feature map.

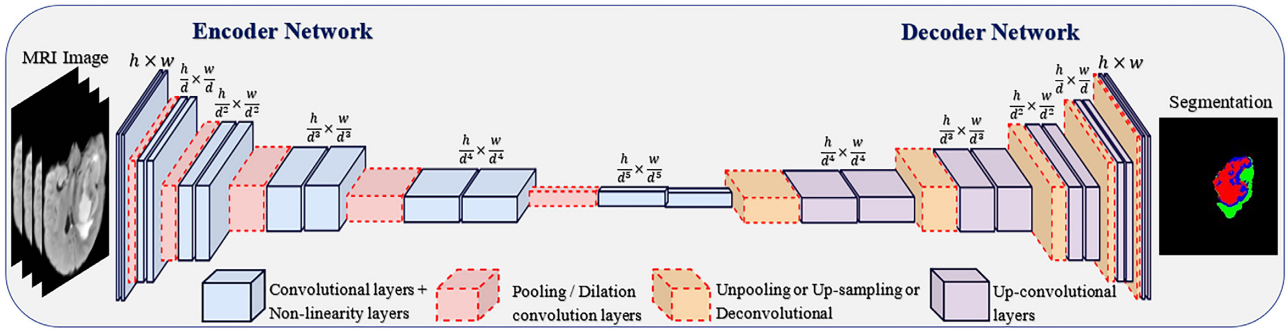


**Figure 12:** The building blocks of a CNNs-based image segmentation. The network architecture contains two phases, encoder and decoder path. Encoder path to extract different numbers of feature maps from the input images depending on the numbers of filters used, and minimize the spatial dimensions of each feature map by pooling operations. Multi-layer decoder path to generate the accurate segmentation map of input proposal. A dense pixel-wise class prediction map is constructed through multiple series of unpooling, deconvolution, and rectification operations, given a feature map representation obtained from the encoder path. Where  $h$  and  $w$  are spatial dimensions, and  $d$  is constant value = 2.

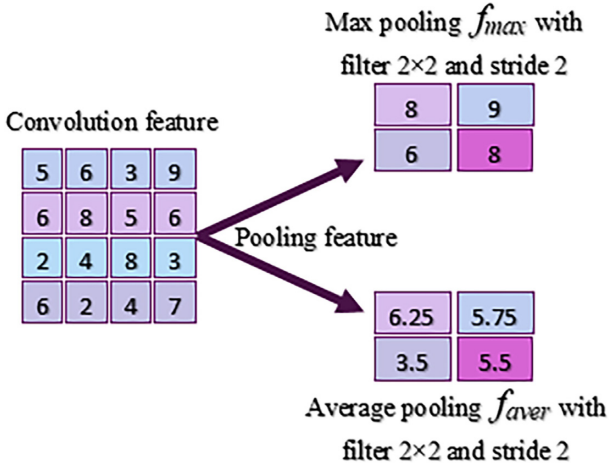


**Figure 13:** Sample of convolution using max and average pooling.

#### 4.1.3. Pooling layers/dilation convolution layers

A pooling layer is often inserted between sequential convolutional layers as a non-linear down-sampling to reduce feature map size and the computation for later layers while keeping important features; specifically, after applying non-linearity and normalization layers. Adding a pooling layer after the convolutional

layer is a common pattern and an important process of ordering layers within an encoder path that may be repeated one or more times in a given model.

The pooling layer operates upon each feature map separately to create a new set of the same number of pooled feature maps. Pooling involves selecting a pooling operation much like a filter to be applied to feature maps and the size of the pooling operation or the filter is smaller than the size of the feature map. Therefore, almost always  $2 \times 2$  pixels are applied with a stride of two pixels. This means, the pooling layer will always reduce the size of each feature map by a factor of 2, and each dimension is halved, reducing the number of pixels, or values in each feature map to one-half the size. For example, a pooling layer applied to a feature map of  $6 \times 6$  (36 pixels) will result in an output pooled feature map of  $3 \times 3$  (nine pixels). The pooling operation is specified rather than learned. Two common functions used in the pooling operation as shown in Fig. 13 are as follows: average pooling:  $f_{\text{aver}}(x_{i,j}) = \frac{1}{N_{(i,j)}} \sum_{i,j=1}^{N_{(i,j)}} x_{i,j}$  calculates the average value for each patch on the feature map (Wang et al., 2017c, 2018b); maximum pooling (or max pooling):  $f_{\text{max}}(x_{i,j}) = \max_{i,j=1}^{N_{(i,j)}} x_{i,j}$  calculates the maximum value for each patch of the feature map (Hang & Aono, 2017; Wang et al., 2018a, b), where the vector  $x$  includes the activation values from a local pooling region of  $N$  pixels (typical pooling region dimensions are  $2 \times 2$  or  $3 \times 3$ ) in an image or a channel (Lee et al., 2018).

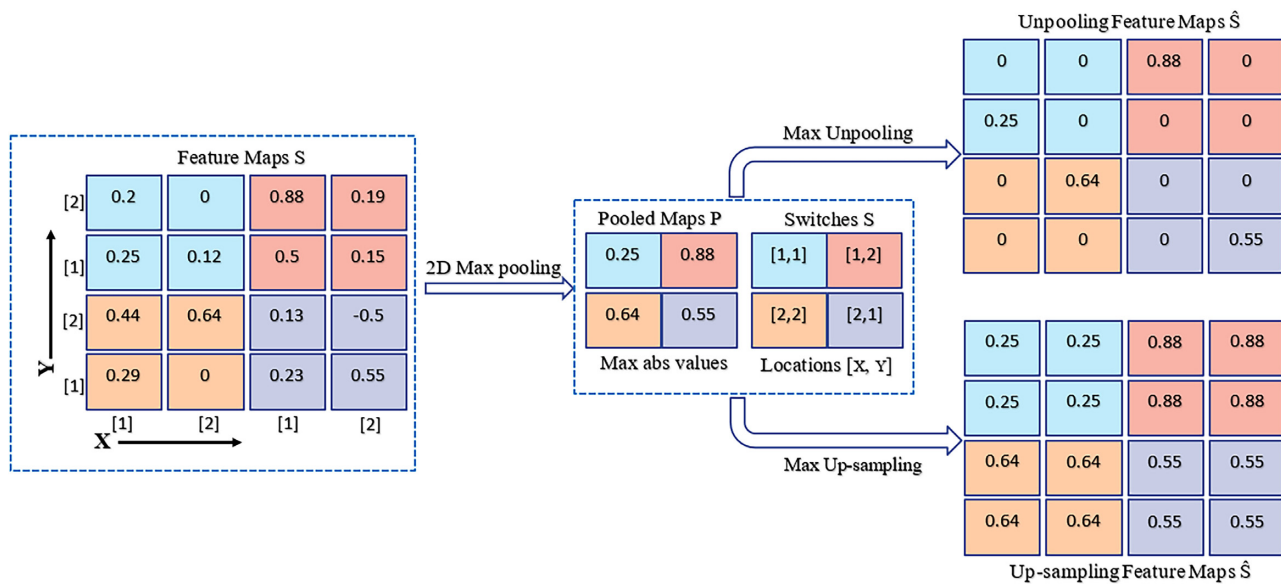


**Figure 14:** Illustration of the unpooling and up-sampling operations in a decoder path. The unpooling operation records the maximum position when performing the max pooling operation and then specifies the position of the maximum value when the reverse process is completed and the sample is filled back to the original position. Unlike unpooling, up-sampling does not need to record the location of the maximum value; this operation directly fills the entire corresponding region with the maximum value obtained by pooling. The switches table records the locations of the maximum value for each pooling layer in an encoder path, where the same color represents the same position between the unpooled feature map and the initial feature map.

The pooling layer is not the only down-sampling method; there are also other layers that do the same tasks, like dilated convolution, that are extremely popular in the field of real-time segmentation. The dilated convolution is proposed by Yu and Koltun (2015) to produce dense prediction, which is used to systematically gather multi-scale contextual information for better segmentation without loss of accuracy. Therefore, dilated convolutions are helpful for pixel-level segmentation tasks.

Dilated convolutions are a type of convolution operator that uses the same filter at different ranges by changing the dilation factor, which allows increasing the size of the receptive field without needing to explore parameters, as well as without increasing computational complexity (Zhang et al., 2019b).

#### 4.2. Decoder network path

The decoder path is identical to the encoder path but hierarchically opposite. All the layers of encoder and decoder path extract feature maps except the last layer of the decoder path which generates pixel-wise class probability maps of the same size as the input image. The major idea of decoder is based on up-sampled the lower resolution input feature maps produced by convolutional layers in the encoder path. The hierarchically of decoder path differs from one architecture to the other depending on the proposed approach.

To reverse the effect of max-pooling operation in order to extend the size of lower resolution input feature maps produced by convolutional layers in the encoder path, we can be used three major operations, this operation is sometimes called backward fractional stride convolution (up-sampling/unpooling) (Long et al., 2015), although it is more commonly known as transposed convolution (Dumoulin & Visin, 2016).

In this path, we discuss two main layers, up-sampling/unpooling and deconvolution layers for segmentation as follows:

##### 4.2.1. Up-sampling/unpooling layers

Usually, the pooling operation is designed to filter noisy activations and retaining only robust activations, which record the location of the maximum value, but the spatial information is lost during pooling. The up-sampling/unpooling layers are used in the decoder path, which implements the reverse operation of pooling and reconstructs the original size of activations as illustrated in Fig. 14.

Unpooling is commonly used in the context of CNNs in decoder path to denote reverse max pooling, we can obtain an approximate inverse by recording the locations of the maximum within each pooling region in a set of switch variables (Zeiler & Fergus, 2014) and retain the spatial information that was lost during pooling operation. In the decoder path, the unpooling operation uses these switches to place the reconstructions from the layer above into appropriate locations, preserving the structure of the stimulus. Whereas the up-sampling layer is a simple layer that will double the dimensions of inputs and followed by traditional convolutional layers.

Typically, every block in the decoder path consists of an up-sampling or unpooling layer (depending on the type of CNNs architecture) of the feature map followed by a  $2 \times 2$  convolution layer “up-convolution” (Ronneberger et al., 2015). This reduces the number of feature channels to halves. Then the reduced feature map is concatenated with the correspondingly cropped feature map from the encoder path.

##### 4.2.2. Deconvolutional layers

Deconvolutional is the inverse process of convolution, also known as transposed convolution. Deconvolutional layer transforms the input in reverse operation of a convolution layer as Fig. 15, but collects new information from the input features map. The deconvolutional layers condense the sparse activations obtained by unpooling through convolution-like operations with multiple

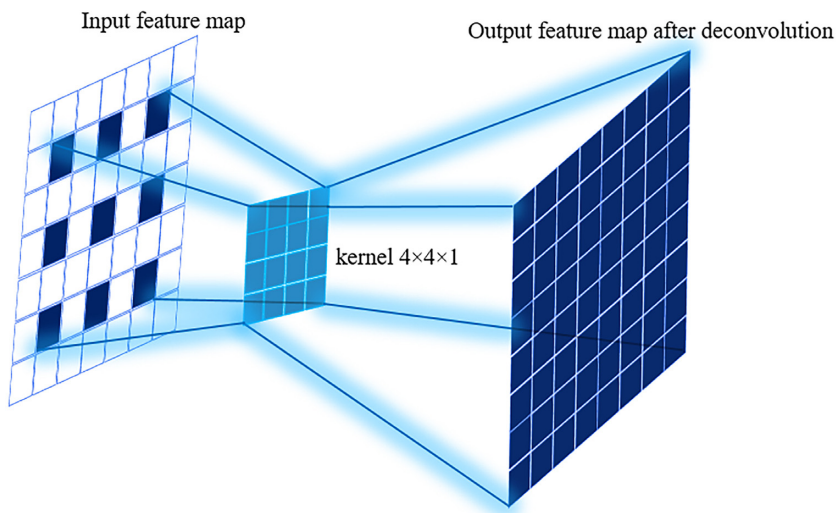


**Figure 15:** Deconvolution operation, the input feature map (left-hand panel) and output feature map (right-hand panel) after deconvolution with kernel =  $4 \times 4$ , stride = 2, and the amount of padding = 0 by doing a full 2D convolution. Raw input size is  $3 \times 3$ , and output size is  $8 \times 8$ .

learned filters. It is used as a mean to up-sample the input feature map toward the resolution of the original input image (Noh et al., 2015; Zeiler et al., 2010). Thus, deconvolutional is carried out in-network for end-to-end learning by backpropagation from the pixel-wise (or voxel-wise in 3D cases) loss (Long et al., 2015), which results in an enlarged and dense activation map. We remove the boundary of the enlarged activation map in order to keep the size of the output map identical to the one from the preceding unpooling layer.

## 5. Conclusions

Inference of tumor regions in brain MRI images remains challenging due to the complexity of brain tumor structure, blurred borders, and external variables. Therefore, in recent years, the accepted standard BraTS datasets have provided a common means for researchers to develop their own methods and evaluate them objectively by using existing techniques (Table 1).

In this survey, we provided an in-depth analysis of the many common techniques used in brain tumor segmentation and discussed the related concepts of brain tumor segmentation methods and the most important contributions in this field, as well as review some recently used segmentation architecture that have the advantage of automatic learning features of the complex features represented for both healthy brain tissues and tumor tissue directly from the modalities MRI images. The different evaluation factors among the state-of-the-art approaches assist in establishing new directions for developing the segmentation techniques and also help with accurate tumor diagnosis in MRI images. In addition, this paper gives a brief overview of MRI modalities and building blocks of CNNs based image segmentation.

In spite of the challenges faced in operations of brain MRI segmentation, deep learning methods can be considered the most recent and commonly used in brain MRI segmentation. Future improvements and modifications in CNNs and segmentation architecture may improve the current segmentation methods, eventually leading to the extraction of complex features and the addition of complementary information from other imaging modalities such as MRS. Future recommendations include similar critical studies of GAN-based methods and its employment in MRI

brain tumor segmentation, which can assist researchers in presenting computer aided diagnostic architecture that will be useful for timely tumor diagnosis.

## Conflict of interest statement

None declared.

## References

- Achanta, R., Shaji, A., Smith, K., Lucchi, A., Fua, P., & Süstrunk, S. (2012). SLIC superpixels compared to state-of-the-art superpixel methods. *IEEE Transactions on Pattern Analysis and Machine Intelligence*, **34**(11), 2274–2282. <https://doi.org/10.1109/TPAMI.2012.120>.
- Adams, R., & Bischof, L. (1994). Seeded region growing. *IEEE Transactions on Pattern Analysis and Machine Intelligence*, **16**(6), 641–647. <https://doi.org/10.1109/34.295913>.
- Agarap, A. F. (2018). Deep learning using Rectified Linear Units (ReLU). *arXiv preprint arXiv:1803.08375*. (1), 2–8. <https://doi.org/10.48550/arXiv.1803.08375>.
- Ahmadvand, A., Yousefi, S., & Manzuri Shalmani, M. T. (2017). A novel Markov random field model based on region adjacency graph for T1 magnetic resonance imaging brain segmentation. *International Journal of Imaging Systems and Technology*, **27**(1), 78–88. <https://doi.org/10.1002/ima.22212>.
- Akselrod-Ballin, A., Galun, M., Gomori, M. J., Basri, R., & Brandt, A. (2006). Atlas guided identification of brain structures by combining 3D segmentation and SVM classification. In *Proceedings of the Medical Image Computing and Computer-Assisted Intervention – MICCAI 2006* (Vol. **4191**, pp. 209–216). Springer. [https://doi.org/10.1007/11866763\\_26](https://doi.org/10.1007/11866763_26).
- Alam, M. S., Rahman, M. M., Hossain, M. A., Islam, M. K., Ahmed, K. M., Ahmed, K. T., Singh, B. C., & Miah, M. S. (2019). Automatic human brain tumor detection in MRI image using template-based K means and improved fuzzy C means clustering algorithm. *Big Data and Cognitive Computing*, **3**(2), 1–18. <https://doi.org/10.3390/bdcc3020027>.
- Al-Faris, A. Q., Ngah, U. K., Isa, N. A. M., & Shuaib, I. L. (2014). Computer-aided segmentation system for breast MRI tumour using modified automatic seeded region growing (BMRI-MASRG).

- Journal of Digital Imaging*, **27**(1), 133–144. <https://doi.org/10.1007/s10278-013-9640-5>.
- Ali, M., Gilani, S. O., Waris, A., Zafar, K., & Jamil, M. (2020). Brain tumour image segmentation using deep networks. *IEEE Access*, **8**, 153589–153598. <https://doi.org/10.1109/ACCESS.2020.3018160>.
- Alipour, N., & Hasanzadeh, R. P. (2021). Superpixel-based brain tumor segmentation in MR images using an extended local fuzzy active contour model. *Multimedia Tools and Applications*, **80**(6), 8835–8859. <https://doi.org/10.1007/s11042-020-10122-1>.
- Ankerst, M., Breunig, M. M., Kriegel, H. P., & Sander, J. (1999). OPTICS: Ordering points to identify the clustering structure. *ACM SIGMOD Record*, **28**(2), 49–60. <https://doi.org/10.1145/304181.304187>.
- Aranguren, I., Valdivia, A., Morales-Castañeda, B., Oliva, D., Abd Elaziz, M., & Perez-Cisneros, M. (2021). Improving the segmentation of magnetic resonance brain images using the LSHADE optimization algorithm. *Biomedical Signal Processing and Control*, **64**, 102259. <https://doi.org/10.1016/j.bspc.2020.102259>.
- Ayachi, R., & Ben Amor, N. (2009). Brain tumor segmentation using support vector machines. In *Lecture notes in computer science* (Vol. **5590**, pp. 736–747). Springer. [https://doi.org/10.1007/978-3-642-02906-6\\_63](https://doi.org/10.1007/978-3-642-02906-6_63).
- Bahadure, N. B., Ray, A. K., & Thethi, H. P. (2017). Image analysis for MRI based brain tumor detection and feature extraction using biologically inspired BWT and SVM. *International Journal of Biomedical Imaging*, **2017**, 9749108. <https://doi.org/10.1155/2017/9749108>.
- Baid, U., Talbar, S., Rane, S., Gupta, S., Thakur, M. H., Moiyadi, A., Sable, N., Akolkar, M., & Mahajan, A. (2020). A novel approach for fully automatic intra-tumor segmentation with 3D U-Net architecture for gliomas. *Frontiers in Computational Neuroscience*, **14**, 1–11. <https://doi.org/10.3389/fncom.2020.00010>.
- Bajwa, I. S., Asghar, M. N., & Naeem, M. A. (2017). Learning-based improved seeded region growing algorithm for brain tumor identification. *Proceedings of the Pakistan Academy of Sciences: Part A*, **54**(2), 127–133.
- Balafar, M. A. (2014). Fuzzy c-mean based brain MRI segmentation algorithms. *Artificial Intelligence Review*, **41**(3), 441–449. <https://doi.org/10.1007/s10462-012-9318-2>.
- Bauer, S., Nolte, L. P., & Reyes, M. (2011). Fully automatic segmentation of brain tumor images using support vector machine classification in combination with hierarchical conditional random field regularization. In *Lecture notes in computer science* (Vol. **6893**, pp. 354–361). Springer. [https://doi.org/10.1007/978-3-642-23626-6\\_44](https://doi.org/10.1007/978-3-642-23626-6_44).
- Bauer, S., Wiest, R., Nolte, L. P., & Reyes, M. (2013). A survey of MRI-based medical image analysis for brain tumor studies. *Physics in Medicine and Biology*, **58**(13), R97–R129. <https://doi.org/10.1088/0031-9155/58/13/R97>.
- Ben naceur, M., Akil, M., Saouli, R., & Kachouri, R. (2020). Fully automatic brain tumor segmentation with deep learning-based selective attention using overlapping patches and multi-class weighted cross-entropy. *Medical Image Analysis*, **63**, 101692. <https://doi.org/10.1016/j.media.2020.101692>.
- Bernal, J., Kushibar, K., Asfaw, D. S., Valverde, S., Oliver, A., Martí, R., & Lladó, X. (2018). Deep convolutional neural networks for brain image analysis on magnetic resonance imaging: A review. *Artificial Intelligence in Medicine*, **95**, 64–81. <https://doi.org/10.1016/j.artmed.2018.08.008>.
- Besag, J. (1975). Statistical analysis of non-lattice data. *Journal of the Royal Statistical Society, Series B*, **24**(3), 179–195. <https://doi.org/10.2307/2987782>.
- Bezdek, J. C., Hall, L. O., & Clarke, L. P. (1993). Review of MR image segmentation techniques using pattern recognition. *Medical Physics*, **20**(4), 1033–1048. <https://doi.org/10.1118/1.597000>.
- Bhandarkar, S. M., Koh, J., & Suk, M. (1997). Multiscale image segmentation using a hierarchical self-organizing map. *Neurocomputing*, **14**(3), 241–272. [https://doi.org/10.1016/S0925-2312\(96\)00048-3](https://doi.org/10.1016/S0925-2312(96)00048-3).
- Bhargavi, K., & Jyothi, S. (2014). A survey on threshold based segmentation technique in image processing. *International Journal of Innovation Research & Development*, **3**(12), 234–239.
- Bhattacharya, M., & Das, A. (2008). A study on seeded region based improved watershed transformation for brain tumor segmentation. In *Proceedings of the XXIX General Assembly of the International Union of Radio Science*. <https://www.academia.edu/50677793>.
- Bleau, A., & Leon, L. J. (2000). Watershed-based segmentation and region merging. *Computer Vision and Image Understanding*, **77**(3), 317–370. <https://doi.org/10.1006/cviu.1999.0822>.
- Bogovic, J. A., Prince, J. L., & Bazin, P. L. (2013). A multiple object geometric deformable model for image segmentation. *Computer Vision and Image Understanding*, **117**(2), 145–157. <https://doi.org/10.1016/j.cviu.2012.10.006>.
- Bora, D. J., & Gupta, A. K. (2014). A comparative study between fuzzy clustering algorithm and hard clustering algorithm. *International Journal of Computer Trends and Technology*, **10**(2), 108–113. <https://doi.org/10.14445/22312803/ijctt-v10p119>.
- Bora, D. J., & Gupta, A. K. (2015). A novel approach towards clustering based image segmentation. *International Journal of Emerging Science and Engineering*, **2**(11), 6–10. <https://doi.org/10.48550/arXiv.1506.01710>.
- Breiman, L. (2001). Random forests. *Machine Learning*, **45**(10), 5–32. <https://doi.org/https://doi.org/10.1023/A:1010933404324>.
- Cahall, D. E., Rasool, G., Bouaynaya, N. C., & Fathallah-Shaykh, H. M. (2021). Dilated inception U-Net (DIU-Net) for brain tumor segmentation. *arXiv*. <https://doi.org/10.48550/arxiv.2108.06772>.
- Campello, R. J., Kröger, P., Sander, J., & Zimek, A. (2020). Density-based clustering. *Wiley Interdisciplinary Reviews: Data Mining and Knowledge Discovery*, **10**(2), 1–15. <https://doi.org/10.1002/widm.1343>.
- Campello, R. J., Moulavi, D., & Sander, J. (2013). Density-based clustering based on hierarchical density estimates. In *Lecture notes in computer science* (Vol. **7819**, pp. 160–172). [https://doi.org/10.1007/978-3-642-37456-2\\_14](https://doi.org/10.1007/978-3-642-37456-2_14).
- Capelle, A. S., Alata, O., Fernandez, C., Lefevre, S., & Ferrie, J. C. (2000). Unsupervised segmentation for automatic detection of brain tumors in MRI. In *Proceedings of the IEEE International Conference on Image Processing* (Vol. **1**, pp. 613–616). <https://doi.org/10.1109/icip.2000.901033>.
- Casamitjana, A., Puch, S., Aduriz, A., & Vilaplana, V. (2017). 3D convolutional neural networks for brain tumor segmentation: A comparison of multi-resolution architectures. *Lecture notes in computer science* (Vol. **10154**, pp. 150–161). <https://doi.org/10.48550/arxiv.1705.08236>.
- Cates, J. E., Whitaker, R. T., & Jones, G. M. (2005). Case study: An evaluation of user-assisted hierarchical watershed segmentation. *Medical Image Analysis*, **9**(6), 566–578. <https://doi.org/10.1016/j.media.2005.04.007>.
- Chan, T., & Vese, L. (2001). Active contours without edges. *IEEE Transactions on Image Processing*, **10**(2), 266–277. <https://doi.org/10.1109/83.902291>.
- Chang, H. H., & Valentino, D. J. (2008). An electrostatic deformable model for medical image segmentation. *Computerized Medical Imaging and Graphics*, **32**(1), 22–35. <https://doi.org/10.1016/j.compmedimag.2007.08.012>.
- Chen, L., Bentley, P., & Rueckert, D. (2017). Fully automatic acute ischemic lesion segmentation in DWI using convolutional neural networks. *NeuroImage: Clinical*, **15**, 633–643. <https://doi.org/10.1016/j.nicl.2017.06.016>.

- Chen, Y., Kalantidis, Y., Li, J., Yan, S., & Feng, J. (2018). Multi-fiber networks for video recognition. In *Lecture notes in computer science* (Vol. 11205). Springer International Publishing.
- Chen, C., Liu, X., Ding, M., Zheng, J., & Li, J. (2019). 3D dilated multi-fiber network for real-time brain tumor segmentation in MRI. In *Lecture notes in computer science* (Vol. 11766, pp. 184–192). [https://doi.org/10.1007/978-3-030-32248-9\\_21](https://doi.org/10.1007/978-3-030-32248-9_21).
- Chen, H., Qin, Z., Ding, Y., Tian, L., & Qin, Z. (2020). Brain tumor segmentation with deep convolutional symmetric neural network. *Neurocomputing*, **392**, 305–313. <https://doi.org/10.1016/j.neucom.2019.01.111>.
- Clevert, D. A., Unterthiner, T., & Hochreiter, S. (2015). Fast and accurate deep network learning by exponential linear units (ELUs). In *Proceedings of the 4th International Conference on Learning Representations, ICLR 2016*. arXiv preprint arXiv:1511.07289. <https://doi.org/10.48550/arxiv.1511.07289>.
- Cunningham, P., & Delany, S. J. (2021). k-Nearest Neighbour Classifiers - A Tutorial. *ACM Computing Surveys (CSUR)*, **54**(6), 1–25. <https://doi.org/10.1145/3459665>.
- Daszykowski, M., & Walczak, B. (2009). Density-based clustering methods. *Comprehensive Chemometrics*, **3**, 635–654. <https://doi.org/10.1016/B978-044452701-1.00067-3>.
- Dilruba, R. A., Chowdhury, N., Liza, F. F., & Karmakar, C. K. (2006). Data pattern recognition using neural network with back-propagation training. In *Proceedings of the 4th International Conference on Electrical and Computer Engineering, ICECE 2006* (pp. 451–455). <https://doi.org/10.1109/ICECE.2006.355667>.
- Drevelegas, A., & Papanikolaou, N. (2011). Imaging modalities in brain tumors. In *Imaging of brain tumors with histological correlations* (pp. 13–33). Springer. <https://doi.org/10.1007/978-3-540-87650-2>.
- Dumoulin, V., & Visin, F. (2016). A guide to convolution arithmetic for deep learning. arXiv:1603.07285. 1–31, <https://doi.org/10.48550/arxiv.1603.07285>.
- Ester, M., Kriegel, H.-P., Sander, J., & Xu, X. (1996). A density-based algorithm for discovering clusters in large spatial databases with noise. *KDD-96 Proceedings*, **96**(34), 226–231.
- Ganesh, M., Naresh, M., & Arvind, C. (2017). MRI brain image segmentation using enhanced adaptive fuzzy k-means algorithm. *Intelligent Automation and Soft Computing*, **23**(2), 325–330. <https://doi.org/10.1080/10798587.2016.1231472>.
- Geman, S., & Geman, D. (1984). Stochastic relaxation, Gibbs distributions, and the Bayesian restoration of images. *IEEE Transactions on Pattern Analysis and Machine Intelligence*, **PAMI-6**(6), 721–741. <https://doi.org/10.1109/TPAMI.1984.4767596>.
- Gies, V., & Bernard, T. M. (2004). Statistical solution to watershed oversegmentation. In *Proceedings of the International Conference on Image Processing, ICIP* (Vol. 3, pp. 1863–1866). <https://doi.org/10.1109/ICIP.2004.1421440>.
- Goetz, M., Weber, C., Binczyk, F., Polanska, J., Tarnawski, R., Bobek-Billewicz, B., Koethe, U., Kleesiek, J., Stieljes, B., & Maier-Hein, K. H. (2016). DALSA: Domain adaptation for supervised learning from sparsely annotated MR images. *IEEE Transactions on Medical Imaging*, **35**(1), 184–196. <https://doi.org/10.1109/TMI.2015.2463078>.
- Gordillo, N., Montseny, E., & Sobrevilla, P. (2013). State of the art survey on MRI brain tumor segmentation. *Magnetic Resonance Imaging*, **31**(8), 1426–1438. <https://doi.org/10.1016/j.mri.2013.05.002>.
- Guan, X., Yang, G., Ye, J., Yang, W., Xu, X., Jiang, W., & Lai, X. (2022). 3D AGSE-VNet: An automatic brain tumor MRI data segmentation framework. *BMC medical imaging*, **22**(1), 6. <https://doi.org/10.1186/S12880-021-00728-8>.
- Guo, D., Fridriksson, J., Fillmore, P., Rorden, C., Yu, H., Zheng, K., & Wang, S. (2015). Automated lesion detection on MRI scans using combined unsupervised and supervised methods. *BMC Medical Imaging*, **15**(1), 1–21. <https://doi.org/10.1186/s12880-015-0092-x>.
- Hamad, Y. A., Simonov, K. V., & Naeem, M. B. (2019). Detection of brain tumor in MRI images, using a combination of fuzzy c-means and thresholding. *International Journal of Advanced Pervasive and Ubiquitous Computing*, **11**(1), 45–60. <https://doi.org/10.4018/ijapuc.2019010104>.
- Hamamci, A., Kucuk, N., Karaman, K., Engin, K., & Unal, G. (2012). Tumor-cut: Segmentation of brain tumors on contrast enhanced MR images for radiosurgery applications. *IEEE Transactions on Medical Imaging*, **31**(3), 790–804. <https://doi.org/10.1109/TMI.2011.2181857>.
- Hang, S. T., & Aono, M. (2017). Bi-linearly weighted fractional max pooling: An extension to conventional max pooling for deep convolutional neural network. *Multimedia Tools and Applications*, **76**(21), 22095–22117. <https://doi.org/10.1007/s11042-017-4840-5>.
- Haralick, R. M., & Shapiro, L. G. (1985). Image segmentation techniques.. *Computer Vision, Graphics, & Image Processing*, **29**(1), 100–132. [https://doi.org/10.1016/S0734-189X\(85\)90153-7](https://doi.org/10.1016/S0734-189X(85)90153-7).
- Havaei, M., Davy, A., Warde-Farley, D., Biard, A., Courville, A., Bengio, Y., Pal, C., Jodoin, P. M., & Larochelle, H. (2017). Brain tumor segmentation with deep neural networks. *Medical Image Analysis*, **35**, 18–31. <https://doi.org/10.1016/j.media.2016.05.004>.
- Havaei, M., Larochelle, H., Poulin, P., & Jodoin, P. M. (2015). Within-brain classification for brain tumor segmentation. *International Journal of Computer Assisted Radiology and Surgery*, **11**(5), 777–788. <https://doi.org/10.1007/s11548-015-1311-1>.
- He, K., Zhang, X., Ren, S., & Sun, J. (2015). Delving deep into rectifiers: Surpassing human-level performance on imagenet classification. In *Proceedings of the IEEE International Conference on Computer Vision* (pp. 1026–1034). <https://doi.org/10.1109/ICCV.2015.123>.
- Hinton, G. (2018). Deep learning – A technology with the potential to transform health care. *JAMA - Journal of the American Medical Association*, **320**(11), 1101–1102. <https://doi.org/10.1001/JAMA.2018.11100>.
- Ho, S., Carolina, N., & Hill, C. (2002). Level-set evolution with region competition: Automatic 3-D segmentation of brain. In *Proceedings of the 2002 International Conference on Pattern Recognition* (pp. 532–535). <https://doi.org/10.1109/ICPR.2002.1044788>.
- Huang, H., Yang, G., Zhang, W., Xu, X., Yang, W., Jiang, W., & Lai, X. (2021). A deep multi-task learning framework for brain tumor segmentation. *Frontiers in Oncology*, **11**, 1–16. <https://doi.org/10.3389/fonc.2021.690244>.
- Hussain, S., Muhammad, S., & Muhammad, M. (2017). Brain tumor segmentation with cascaded deep convolutional neural network. In *Proceedings of the 2017 39th Annual International Conference of the IEEE Engineering in Medicine and Biology Society (EMBC)* (pp. 1998–2001). <https://doi.org/10.1109/EMBC.2017.8037243>.
- Ilhan, U., & Ilhan, A. (2017). Brain tumor segmentation based on a new threshold approach. *Procedia Computer Science*, **120**, 580–587. <https://doi.org/10.1016/J.PROCS.2017.11.282>.
- Ilunga-Mbuyamba, E., Cruz-Duarte, J. M., Avina-Cervantes, J. G., Correa-Cely, C. R., Lindner, D., & Chalopin, C. (2016). Active contours driven by cuckoo search strategy for brain tumour images segmentation. *Expert Systems with Applications*, **56**, 59–68. <https://doi.org/10.1016/j.eswa.2016.02.048>.
- Imtiaz, T., Rifat, S., Fattah, S. A., & Wahid, K. A. (2020). Automated brain tumor segmentation based on multi-planar superpixel level features extracted from 3D MR images. *IEEE Access*, **8**, 25335–25349. <https://doi.org/10.1109/ACCESS.2019.2961630>.
- İşin, A., Direkoglu, C., & Şah, M. (2016). Review of MRI-based brain tumor image segmentation using deep learning methods. *Procedia*

- Computer Science, **102**, 317–324. <https://doi.org/10.1016/j.procs.2016.09.407>.
- Jiang, Z., Ding, C., Liu, M., & Tao, D. (2020). Two-stage cascaded U-Net: 1st place solution to BraTS challenge 2019 segmentation task. In *Brainlesion: Glioma, multiple sclerosis, stroke and traumatic brain injuries* (Vol. **11992**, pp. 231–241). Springer International Publishing.
- Jiang, Y., Ye, M., Wang, P., Huang, D., & Lu, X. (2022). MRF-IUNet: A multi-resolution fusion brain tumor segmentation network based on improved inception U-Net. *Computational and Mathematical Methods in Medicine*, **2022**, 6305748. <https://doi.org/10.1155/2022/6305748>.
- Jiji, G. W., & Ganesan, L. (2007). Unsupervised segmentation using fuzzy logic based texture spectrum for MRI brain images. *International Journal of Medical and Health Sciences*, **1**(5), 317–319.
- Juang, L. H., & Wu, M. N. (2010). MRI brain lesion image detection based on color-converted k-means clustering segmentation. *Measurement: Journal of the International Measurement Confederation*, **43**(7), 941–949. <https://doi.org/10.1016/j.measurement.2010.03.013>.
- Kamnitsas, K., Bai, W., Ferrante, E., McDonagh, S., Sinclair, M., Pawlowski, N., Rajchl, M., Lee, M., Kainz, B., Rueckert, D., & Glocker, B. (2018). Ensembles of multiple models and architectures for robust brain tumour segmentation. In *Lecture notes in computer science* (Vol. **10670**, pp. 450–462). [https://doi.org/10.1007/978-3-319-75238-9\\_38](https://doi.org/10.1007/978-3-319-75238-9_38).
- Kamnitsas, K., Chen, L.-C., Ledig, C., Rueckert, D., & Glocker, B. (2015). Multi-scale 3D convolutional neural networks for lesion segmentation in brain MRI. In *Proceedings of the MICCAI-ISLES 2015* (pp. 13–16).
- Kamnitsas, K., Enzo, F., Sarah, P., Christian, L., Aditya V, N., Antonio, C., Daniel, R., & Ben, G. (2017a). DeepMedic for brain tumor segmentation (Vol. **10154**, pp. 138–149). Springer. [https://doi.org/10.1007/978-3-319-55524-9\\_14](https://doi.org/10.1007/978-3-319-55524-9_14).
- Kamnitsas, K., Ledig, C., Newcombe, V. F., Simpson, J. P., Kane, A. D., Menon, D. K., Rueckert, D., & Glocker, B. (2017b). Efficient multi-scale 3D CNN with fully connected CRF for accurate brain lesion segmentation. *Medical Image Analysis*, **36**(2), 61–78. <https://doi.org/10.1016/j.media.2016.10.004>.
- Kang, D., Shin, S. Y., Sung, C. O., Kim, J. Y., Pack, J. K., & Choi, H. D. (2011). An improved method of breast MRI segmentation with simplified k-means clustered images. In *Proceedings of the 2011 ACM Research in Applied Computation Symposium, RACS 2011* (pp. 226–231). <https://doi.org/10.1145/2103380.2103425>.
- Kang, W. X., Yang, Q. Q., & Liang, R. P. (2009). The comparative research on image segmentation algorithms. In *Proceedings of the 1st International Workshop on Education Technology and Computer Science, ETCS 2009* (Vol. **2**, pp. 703–707). <https://doi.org/10.1109/ETCS.2009.417>.
- Karayegen, G., & Aksahin, M. F. (2021). Brain tumor prediction on MR images with semantic segmentation by using deep learning network and 3D imaging of tumor region. *Biomedical Signal Processing and Control*, **66**, 102458. <https://doi.org/10.1016/j.bspc.2021.102458>.
- Karthik, R., Gupta, U., Jha, A., Rajalakshmi, R., & Menaka, R. (2019). A deep supervised approach for ischemic lesion segmentation from multimodal MRI using fully convolutional network. *Applied Soft Computing*, **84**, 105685. <https://doi.org/10.1016/j.asoc.2019.105685>.
- Kaus, M. R., Warfield, S. K., Nabavi, A., Black, P. M., Jolesz, F. A., & Kikinis, R. (2001). Automated segmentation of MR images of brain tumors. *Radiology*, **218**(2), 586–591. <https://doi.org/10.1148/radiology.218.2.r01fe44586>.
- Kavitha, A. R., Chellamuthu, C., & Rupa, K. (2012). An efficient approach for brain tumour detection based on modified region growing and neural network in MRI images. In *Proceedings of the 2012 International Conference on Computing, Electronics and Electrical Technologies, ICCEET 2012* (pp. 1087–1095). <https://doi.org/10.1109/ICCEET.2012.6203809>.
- Ke, Q., Liu, J., Bennamoun, M., An, S., Sohel, F., & Boussaid, F. (2018). Computer vision for human-machine interaction. In *Computer vision for assistive healthcare* (pp. 127–145). Elsevier Ltd.
- Kharrat, A., Gasmi, K., Ben Messaoud, M., Benamrane, N., & Abid, M. (2010). A hybrid approach for automatic classification of brain MRI using genetic algorithm and support vector machine. *Leonardo Journal of Sciences*, **17**, 71–82.
- Kichenassamy, S., Kumar, A., Olver, P., Tannenbaum, A., & Yezzi, A. (1995). Gradient flows and geometric active contour models. In *Proceedings of the IEEE International Conference on Computer Vision* (pp. 810–815). <https://doi.org/10.1109/iccv.1995.466855>.
- Kohonen, T. (1982). Self-organized formation of topologically correct feature maps. *Biological Cybernetics*, **43**(1), 59–69. <https://doi.org/10.1007/BF00337288>.
- Koley, S., Sadhu, A. K., Mitra, P., Chakraborty, B., & Chakraborty, C. (2016). Delineation and diagnosis of brain tumors from post contrast T1-weighted MR images using rough granular computing and random forest. *Applied Soft Computing Journal*, **41**, 453–465. <https://doi.org/10.1016/j.asoc.2016.01.022>.
- Kuo, W. F., Lin, C. Y., & Sun, Y. N. (2008). Brain MR images segmentation using statistical ratio: Mapping between watershed and competitive Hopfield clustering network algorithms. *Computer Methods and Programs in Biomedicine*, **91**(3), 191–198. <https://doi.org/10.1016/j.cmpb.2008.04.010>.
- Kwon, D., Shinohara, R. T., Akbari, H., & Davatzikos, C. (2014). Combining generative models for multifocal glioma segmentation and registration. In *Lecture notes in computer science* (Vol. **8673**, pp. 763–770). [https://doi.org/10.1007/978-3-319-10404-1\\_95](https://doi.org/10.1007/978-3-319-10404-1_95).
- Lafferty, J., McCallum, A., & Pereira, F. C. (2001). Conditional random fields: Probabilistic models for segmenting and labeling sequence data. In *Proceedings of the 18th International Conference on Machine Learning 2001 (ICML 2001)*.
- Lakare, S. (2000). 3D segmentation techniques for medical volumes. *Neural Networks*, **65**, 1–23.
- Lecun, Y., Bengio, Y., & Hinton, G. (2015). Deep learning. *Nature*, **521**(7553), 436–444. <https://doi.org/10.1038/nature14539>.
- Lee, C.-Y., Gallagher, P., & Tu, Z. (2018). Generalizing pooling functions in CNNs: Mixed, gated, and tree. *IEEE Transactions on Pattern Analysis and Machine Intelligence*, **40**(4), 863–875. <https://doi.org/10.1109/TPAMI.2017.2703082>.
- Lee, C. H., Schmidt, M., Murtha, A., Bistritz, A., Sander, J., & Greiner, R. (2005). Segmenting brain tumors with conditional random fields and support vector machines. In *Computer Vision for Biomedical Image Applications. CVBIA 2005. Lecture Notes in Computer Science* (Vol. **3765**, pp. 469–478). [https://doi.org/10.1007/11569541\\_47](https://doi.org/10.1007/11569541_47).
- Li, B. N., Chui, C. K., Chang, S., & Ong, S. H. (2011). Integrating spatial fuzzy clustering with level set methods for automated medical image segmentation. *Computers in Biology and Medicine*, **41**(1), 1–10. <https://doi.org/10.1016/j.combiomed.2010.10.007>.
- Li, C., Kao, C. Y., Gore, J. C., & Ding, Z. (2008). Minimization of region-scalable fitting energy for image segmentation. *IEEE Transactions on Image Processing*, **17**(10), 1940–1949. <https://doi.org/10.1109/TIP.2008.2002304>.
- Li, H., Li, A., & Wang, M. (2019). A novel end-to-end brain tumor segmentation method using improved fully convolutional networks. *Computers in Biology and Medicine*, **108**, 150–160. <https://doi.org/10.1016/j.combiomed.2019.03.014>.

- Li, N., Liu, M., & Li, Y. (2007). Image segmentation algorithm using watershed transform and level set method. In *Proceedings of the IEEE International Conference on Acoustics, Speech and Signal Processing - ICASSP* (Vol. 1, pp. 613–616). <https://doi.org/10.1109/ICASSP.2007.365982>.
- Liu, J., & Guo, L. (2015). A new brain MRI image segmentation strategy based on k-means clustering and SVM. In *Proceedings of the 2015 7th International Conference on Intelligent Human-Machine Systems and Cybernetics* (Vol. 2, pp. 270–273). <https://doi.org/10.1109/IHMSC.2015.182>.
- Liu, J., Li, M., Wang, J., Wu, F., Liu, T., & Pan, Y. (2014). A survey of MRI-based brain tumor segmentation methods. *Tsinghua Science and Technology*, **19**(6), 578–595. <https://doi.org/10.1109/TST.2014.6961028>.
- Lok, K. H., Shi, L., Zhu, X., & Wang, D. (2017). Fast and robust brain tumor segmentation using level set method with multiple image information. *Journal of X-Ray Science and Technology*, **25**(2), 301–312. <https://doi.org/10.3233/XST-17261>.
- Long, J., Shelhamer, E., & Darrell, T. (2015). Fully convolutional networks for semantic segmentation. In *Proceedings of the 2015 IEEE Conference on Computer Vision and Pattern Recognition (CVPR)* (pp. 3431–3440).
- Lundervold, A. S., & Lundervold, A. (2019). An overview of deep learning in medical imaging focusing on MRI. *Zeitschrift für Medizinische Physik*, **29**(2), 102–127. <https://doi.org/10.1016/j.zemedi.2018.11.002>.
- Maas, A. L., Hannun, A. Y., & Ng, A. Y. (2013). Rectifier nonlinearities improve neural network acoustic models. In *Proceedings of the 30th International Conference on Machine Learning* (Vol. 30, p. 3).
- Maier, O., Schröder, C., Forkert, N. D., Martinetz, T., & Handels, H. (2015). Classifiers for ischemic stroke lesion segmentation: A comparison study. *PLoS ONE*, **10**(12), 1–16. <https://doi.org/10.1371/journal.pone.0145118>.
- Malladi, R., Sethian, J. A., & Vemuri, B. C. (1995). Shape modeling with front propagation: A level set approach. *IEEE Transactions on Pattern Analysis and Machine Intelligence*, **17**(2), 158–175. <https://doi.org/10.1109/34.368173>.
- Marroquin, J. L., Vemuri, B. C., Botello, S., & Calderon, F. (2002). An accurate and efficient Bayesian method for automatic segmentation of brain MRI. *IEEE Transactions on Medical Imaging*, **21**(8), 934–945. <https://doi.org/10.1109/TMI.2002.803119>.
- Meier, R., Knecht, U., Loosli, T., Bauer, S., Slotboom, J., Wiest, R., & Reyes, M. (2016). Clinical evaluation of a fully-automatic segmentation method for longitudinal brain tumor volumetry. *Scientific Reports*, **6**, 1–11. <https://doi.org/10.1038/srep23376>.
- Menze, B. H. et al. (2015). The multimodal brain tumor image segmentation benchmark (Brats). *IEEE Transactions on Medical Imaging*, **34**(10), 1993–2024. <https://doi.org/10.1109/TMI.2014.2377694>.
- Milletari, F., Navab, N., & Ahmadi, S. A. (2016). V-Net: Fully convolutional neural networks for volumetric medical image segmentation. In *Proceedings of the 2016 4th International Conference on 3D Vision, 3DV 2016* (pp. 565–571). <https://doi.org/10.1109/3DV.2016.79>.
- Moeskops, P., Viergever, M. A., Mendrik, A. M., De Vries, L. S., Benders, M. J., & Isgum, I. (2016). Automatic segmentation of MR brain images with a convolutional neural network. *IEEE Transactions on Medical Imaging*, **35**(5), 1252–1261. <https://doi.org/10.1109/TMI.2016.2548501>.
- Moher, D., Liberati, A., Tetzlaff, J., & Altman, D. G. (2010). Preferred reporting items for systematic reviews and meta-analyses: The PRISMA statement. *International Journal of Surgery*, **8**(5), 336–341. <https://doi.org/10.1016/j.ijssu.2010.02.007>.
- Montazer, G. A., & Giveki, D. (2015). An improved radial basis function neural network for object image retrieval. *Neurocomputing*, **168**, 221–233. <https://doi.org/10.1016/j.neucom.2015.05.104>.
- Naceur, M. B., Saouli, R., Akil, M., & Kachouri, R. (2018). Fully automatic brain tumor segmentation using end-to-end incremental deep neural networks in MRI images. *Computer Methods and Programs in Biomedicine*, **166**, 39–49. <https://doi.org/10.1016/j.cmpb.2018.09.007>.
- Noh, H., Hong, S., & Han, B. (2015). Learning deconvolution network for semantic segmentation. In *Proceedings of the IEEE International Conference on Computer Vision (Vol. 2015 Inter*, pp. 1520–1528). <https://doi.org/10.1109/ICCV.2015.178>.
- Nyma, A., Kang, M., Kwon, Y. K., Kim, C. H., & Kim, J. M. (2012). A hybrid technique for medical image segmentation. *Journal of Biomedicine and Biotechnology*, **2012**, 830252. <https://doi.org/10.1155/2012/830252>.
- Nyúl, L. G., Udupa, J. K., & Zhang, X. (2000). New variants of a method of MRI scale standardization. *IEEE Transactions on Medical Imaging*, **19**(2), 143–150. <https://doi.org/10.1109/42.836373>.
- Page, M. J. et al. (2021). The PRISMA 2020 statement: An updated guideline for reporting systematic reviews. *Systematic Reviews*, **10**(1), 1–11. <https://doi.org/10.1186/s13643-021-01626-4>.
- Parveen, , & Singh, A. (2015). Detection of brain tumor in MRI images, using combination of fuzzy c-means and SVM. In *Proceedings of the 2nd International Conference on Signal Processing and Integrated Networks, SPIN 2015* (pp. 98–102). <https://doi.org/10.1109/SPIN.2015.7095308>.
- Pereira, S., Oliveira, A., Alves, V., & Silva, C. A. (2017). On hierarchical brain tumor segmentation in MRI using fully convolutional neural networks: A preliminary study. In *Proceedings of the 2017-5th Portuguese Meeting on Bioengineering, ENBENG 2017* (pp. 1–4). <https://doi.org/10.1109/ENBENG.2017.7889452>.
- Pereira, S., Pinto, A., Alves, V., & Silva, C. A. (2016). Brain tumor segmentation using convolutional neural networks in MRI images. *IEEE Transactions on Medical Imaging*, **35**(5), 1240–1251. <https://doi.org/10.1109/TMI.2016.2538465>.
- Pham, D. T., Dimov, S. S., & Nguyen, C. D. (2005). Selection of k in k-means clustering. *Proceedings of the Institution of Mechanical Engineers, Part C: Journal of Mechanical Engineering Science*, **219**(1), 103–119. <https://doi.org/10.1243/095440605X8298>.
- Popuri, K., Cobzas, D., Jagersand, M., Shah, S. L., & Murtha, A. (2009). 3D variational brain tumor segmentation on a clustered feature set. In *Proceedings of the SPIE, Medical Imaging 2009: Image Processing*, (Vol. **7259**, pp. 562–571). <https://doi.org/10.1117/12.811029>.
- Preim, B., & Botha, C. (2014). Image analysis for medical visualization. *Visual Computing for Medicine*, **2014**, 111–175. <https://doi.org/10.1016/b978-0-12-415873-3.00004-3>.
- Quteishat, A., Al-Batah, M., Al-Mofleh, A., & Alnabelsi, S. H. (2013). Cervical cancer diagnostic system using adaptive fuzzy moving k-means algorithm and fuzzy min-max neural network. *Journal of Theoretical and Applied Information Technology*, **57**(1), 48–53.
- Rabeh, A. B., Benzarti, F., & Amiri, H. (2017). Segmentation of brain MRI using active contour model. *International Journal of Imaging Systems and Technology*, **27**(1), 3–11. <https://doi.org/10.1002/ima.2205>.
- Rajendran, A., & Dhanasekaran, R. (2012). Fuzzy clustering and deformable model for tumor segmentation on MRI brain image: A combined approach. *Procedia Engineering*, **30**, 327–333. <https://doi.org/10.1016/j.proeng.2012.01.868>.
- Ramteke, R. J., & Monali, K. (2012). Automatic medical image classification and abnormality detection using K-nearest neighbour. *International Journal of Advanced Computer Research*, **2**(4), 190–196.

- Ranjbarzadeh, R., Bagherian Kasgari, A., Jafarzadeh Ghoushchi, S., Anari, S., Naseri, M., & Bendechache, M. (2021). Brain tumor segmentation based on deep learning and an attention mechanism using MRI multi-modalities brain images. *Scientific Reports*, **11**(1), 1–17. <https://doi.org/10.1038/s41598-021-90428-8>.
- Raschke, F., Barrick, T. R., Jones, T. L., Yang, G., Ye, X., & Howe, F. A. (2019). Tissue-type mapping of gliomas. *NeuroImage: Clinical*, **21**, 101648. <https://doi.org/10.1016/j.nicl.2018.101648>.
- Ratan, R., Sharma, S., & Sharma, S. K. (2009). Multiparameter segmentation and quantization of brain tumor from MRI images. *Indian Journal of Science and Technology*, **2**(2), 11–15. <https://doi.org/10.17485/ijst/2009/v2i2/29385>.
- Rehman, M. U., Cho, S., Kim, J. H., & Chong, K. T. (2020). Bu-Net: Brain tumor segmentation using modified U-Net architecture. *Electronics (Switzerland)*, **9**(12), 1–12. <https://doi.org/10.3390/electronics9122203>.
- Rehman, M. U., Cho, S., Kim, J., & Chong, K. T. (2021). BrainSegNet: Brain tumor MR image segmentation via enhanced encoder-decoder network. *Diagnostics*, **11**(2), 169. <https://doi.org/10.3390/diagnostics11020169>.
- Rogowska, J. (2000). Overview and fundamentals of medical image segmentation. In *Handbook of medical imaging* (pp. 69–85). <https://doi.org/10.1016/b978-012077790-7/50009-6>.
- Ronneberger, O., Fischer, P., & Brox, T. (2015). U-Net: Convolutional networks for biomedical image segmentation. In *Proceedings of the Medical Image Computing and Computer-Assisted Intervention – MICCAI 2015* (Vol. **9351**, pp. 234–241). Springer. [https://doi.org/10.1007/978-3-319-24574-4\\_28](https://doi.org/10.1007/978-3-319-24574-4_28).
- Safavian, N., Batouli, S. A. H., & Oghabian, M. A. (2020). An automatic level set method for hippocampus segmentation in MR images. *Computer Methods in Biomechanics and Biomedical Engineering: Imaging and Visualization*, **8**(4), 400–410. <https://doi.org/10.1080/21681163.2019.1706054>.
- Salman, Y. M., Assal, M. A., Badawi, A. M., Alian, S. M., & El-Bayome, M. E. M. (2005a). Validation techniques for quantitative brain tumors measurements. In *Proceedings of the Annual International Conference of the IEEE Engineering in Medicine and Biology* (Vol. **7**, pp. 7048–7051). <https://doi.org/10.1109/embc.2005.1616129>.
- Salman, Y. M., Assal, M. A., Badawi, A. M., Alian, S. M., & El-Bayumoi, M. (2005b). New automatic technique for tracking brain tumor response. In *Proceedings of the International Conference on Biological and Medical Physics* (Vol. **c**, p. 2005).
- Saman, S., & Jamjala Narayanan, S. (2019). Survey on brain tumor segmentation and feature extraction of MR images. *International Journal of Multimedia Information Retrieval*, **8**(2), 79–99. <https://doi.org/10.1007/s13735-018-0162-2>.
- Sánchez, C. I., Ghafoorian, M., Kooi, T., Ciompi, F., Litjens, G., Bejnordi, B. E., Setio, A. A. A., van der Laak, J. A., & van Ginneken, B. (2017). A survey on deep learning in medical image analysis. *Medical Image Analysis*, **42**, 60–88. <https://doi.org/10.1016/j.media.2017.07.005>.
- Sandabad, S., Benba, A., Tahri, Y. S., & Hammouch, A. (2016). Novel extraction and tumour detection method using histogram study and SVM classification. *International Journal of Signal and Imaging Systems Engineering*, **9**(4/5), 202–208. <https://doi.org/10.1504/IJSISE.2016.078262>.
- Sandhya, G., Kande, G. B., & Savithri, T. S. (2020). Tumor segmentation by a self-organizing-map based active contour model (SOMACM) from the brain MRIs. *IETE Journal of Research*, **68**(6), 3927–3939. <https://doi.org/10.1080/03772063.2020.1782780>.
- Sathies Kumar, T., Rashmi, K., Ramadoss, S., Sandhya, L. K., & Sangeetha, T. J. (2017). Brain tumor detection using SVM classifier. In *Proceedings of 2017 3rd IEEE International Conference on Sensors and Smart Systems* (pp. 318–323). <https://doi.org/10.1109/SSPS.2017.8071613>.
- Sato, M., Lakare, S., Wan, M., & Kaufman, A. (2000). A gradient magnitude based region growing algorithm for accurate segmentation. In *Proceedings of the 2000 International Conference on Image Processing (Cat. No.00CH37101)* (pp. 448–451). <https://doi.org/10.1109/ICIP.2000.899432>.
- Schmidl, W. F., Raudys, S., Kraaijveldl, M. A., Skurikhina, M., & Duin, R. P. W. (1993). Initializations, back-propagation and generalization of feed-forward classifiers. In *Proceedings of the IEEE International Conference on Neural Networks* (Vol. **1**, pp. 598–604). <https://doi.org/10.1109/ICNN.1993.298625>.
- Seo, H., Yu, L., Ren, H., Li, X., Shen, L., & Xing, L. (2021). Deep neural network with consistency regularization of multi-output channels for improved tumor detection and delineation. *IEEE Transactions on Medical Imaging*, **40**(12), 3369–3378. <https://doi.org/10.1109/TMI.2021.3084748>.
- Setyawan, R., Almahfud, M. A., Sari, C. A., Setiadi, D. R. I. M., & Rachmawanto, E. H. (2018). MRI image segmentation using morphological enhancement and noise removal based on fuzzy c-means. In *Proceedings of the 2018 5th International Conference on Information Technology, Computer and Electrical Engineering, ICITACEE 2018* (pp. 99–104). <https://doi.org/10.1109/ICITACEE.2018.8576941>.
- Sharma, S., Sharma, S., & Athaiya, A. (2020). Activation functions in neural networks. *International Journal of Engineering Applied Sciences and Technology*, **4**(12), 310–316.
- Simonyan, K., & Zisserman, A. (2015). Very deep convolutional networks for large-scale image recognition. In *Proceedings of the 3rd International Conference on Learning Representations, ICLR 2015* (pp. 1–14). <https://doi.org/10.48550/arXiv.1409.1556>.
- Soltaninejad, M., Yang, G., Lambrou, T., Allinson, N., Jones, T. L., Barrick, T. R., Howe, F. A., & Ye, X. (2017). Automated brain tumour detection and segmentation using superpixel-based extremely randomized trees in FLAIR MRI. *International Journal of Computer Assisted Radiology and Surgery*, **12**(2), 183–203. <https://doi.org/10.1007/S11548-016-1483-3>.
- Soltaninejad, M., Yang, G., Lambrou, T., Allinson, N., Jones, T. L., Barrick, T. R., Howe, F. A., & Ye, X. (2018a). Supervised learning based multimodal MRI brain tumour segmentation using texture features from supervoxels. *Computer Methods and Programs in Biomedicine*, **157**, 69–84. <https://doi.org/10.1016/j.cmpb.2018.01.003>.
- Soltaninejad, M., Zhang, L., Lambrou, T., Yang, G., Allinson, N., & Ye, X. (2018b). MRI brain tumor segmentation and patient survival prediction using random forests and fully convolutional networks. In *Lecture notes in computer science* (Vol. **10670**, pp. 204–215). [https://doi.org/10.1007/978-3-319-75238-9\\_18](https://doi.org/10.1007/978-3-319-75238-9_18).
- Sonoda, S., & Murata, N. (2017). Neural network with unbounded activation functions is universal approximator. *Applied and Computational Harmonic Analysis*, **43**(2), 233–268. <https://doi.org/10.1016/JACHA.2015.12.005>.
- Sornam, M., & Devi, M. P. (2015). A survey on back propagation neural network. *International Journal of Communication and Networking System*, **5**(1), 70–74. <https://doi.org/10.20894/ijcnes.103.005.001.019>.
- Stutz, D., Hermans, A., & Leibe, B. (2018). Superpixels: An evaluation of the state-of-the-art. *Computer Vision and Image Understanding*, **166**, 1–27. <https://doi.org/10.1016/j.cviu.2017.03.007>.
- Su, P., Yang, J., Li, H., Chi, L., Xue, Z., & Wong, S. T. (2013). Superpixel-based segmentation of glioblastoma multiforme from multi-modal MR images. In *Lecture notes in computer science* (Vol. **8159 LNCS**, pp. 74–83). [https://doi.org/10.1007/978-3-319-02126-3\\_8](https://doi.org/10.1007/978-3-319-02126-3_8).
- Sujan, M., Alam, N., Abdullah, S., & Jahirul, M. (2016). A segmentation based automated system for brain tumor detection. *International Journal of Image Processing*, **2**(1), 1–10. <https://doi.org/10.1109/ijip.2016.7500001>.

- Journal of Computer Applications, **153**(10), 41–49. <https://doi.org/10.5120/ijca2016912171>.
- Sultana, F., Sufian, A., & Dutta, P. (2020). Evolution of image segmentation using deep convolutional neural network: A survey. *Knowledge-Based Systems*, **201-202**, 1–38. <https://doi.org/10.1016/j.knosys.2020.106062>.
- Sun, J., Peng, Y., Guo, Y., & Li, D. (2021). Segmentation of the multimodal brain tumor image used the multi-pathway architecture method based on 3D FCN. *Neurocomputing*, **423**, 34–45. <https://doi.org/10.1016/j.neucom.2020.10.031>.
- Suthaharan, S. (2016). Support vector machine. *Machine Learning Models and Algorithms for Big Data Classification*, **36**, 207–235. [https://doi.org/10.1007/978-1-4899-7641-3\\_9](https://doi.org/10.1007/978-1-4899-7641-3_9).
- Szegedy, C., Wei, Liu, Yangqing, Jia, Sermanet, P., Reed, S., Anguelov, D., Erhan, D., Vanhoucke, V., & Rabinovich, A. (2015). Going deeper with convolutions. In *Proceedings of the 2015 IEEE Conference on Computer Vision and Pattern Recognition (CVPR)* (pp. 1–9). IEEE.
- Tarkhaneh, O., & Shen, H. (2019). An adaptive differential evolution algorithm to optimal multi-level thresholding for MRI brain image segmentation. *Expert Systems with Applications*, **138**, 112820. <https://doi.org/10.1016/j.eswa.2019.07.037>.
- Thaha, M. M., Kumar, K. P. M., Murugan, B. S., Dhanasekeran, S., Vijayakarthick, P., & Selvi, A. S. (2019). Brain tumor segmentation using convolutional neural networks in MRI images. *Journal of Medical Systems*, **43**(9), 294. <https://doi.org/10.1007/s10916-019-1416-0>.
- Tran, T. N., Wehrens, R., & Buydens, L. M. (2005). Clustering multispectral images: A tutorial. *Chemometrics and Intelligent Laboratory Systems*, **77**(1–2), 3–17. <https://doi.org/10.1016/j.chemolab.2004.07.011>.
- Tripathi, S., Anand, R. S., & Fernandez, E. (2018). A review of brain MR image segmentation techniques. *International Journal of Research and Analytical Reviews*, **5**(2), 1295.
- Tustison, N. J., Avants, B. B., Cook, P. A., Zheng, Y., Egan, A., Yushkevich, P. A., & Gee, J. C. (2010). N4ITK: Improved N3 bias correction. *IEEE Transactions on Medical Imaging*, **29**(6), 1310–1320. <https://doi.org/10.1109/TMI.2010.2046908>.
- Vaibhavi, P., & Rupal, K. (2018). *Brain tumor segmentation using k-means-FCM hybrid technique* (Vol. **696**). Springer.
- Vapnik, V. N. (1999). An overview of statistical learning theory. *IEEE Transactions on Neural Networks*, **10**(5), 988–999. <https://doi.org/10.1109/72.788640>.
- Vijay, J., & Subhashini, J. (2013). An efficient brain tumor detection methodology using k-means clustering algoriftnn. In *Proceedings of the International Conference on Communication and Signal Processing, ICCSP 2013* (pp. 653–657). <https://doi.org/10.1109/iccsp.2013.6577136>.
- Vijayakumar, C., Damayanti, G., Pant, R., & Sreedhar, C. M. (2007). Segmentation and grading of brain tumors on apparent diffusion coefficient images using self-organizing maps. *Computerized Medical Imaging and Graphics*, **31**(7), 473–484. <https://doi.org/10.1016/j.commpmedimag.2007.04.004>.
- Virupakshappa, & Amarapur, B. (2019). Cognition-based MRI brain tumor segmentation technique using modified level set method. *Cognition, Technology and Work*, **21**(3), 357–369. <https://doi.org/10.1007/s10111-018-0472-4>.
- Wadhwa, A., Bhardwaj, A., & Singh Verma, V. (2019). A review on brain tumor segmentation of MRI images. *Magnetic Resonance Imaging*, **61**, 247–259. <https://doi.org/10.1016/j.mri.2019.05.043>.
- Wang, J., Gao, J., Ren, J., Luan, Z., Yu, Z., Zhao, Y., & Zhao, Y. (2021). DFP-ResUNet: Convolutional neural network with a dilated convolutional feature pyramid for multimodal brain tumor segmen-
- tation. *Computer Methods and Programs in Biomedicine*, **208**, 106208. <https://doi.org/10.1016/j.cmpb.2021.106208>.
- Wang, S., Jiang, Y., Hou, X., Cheng, H., & Du, S. (2017c). Cerebral microbleed detection based on the convolution neural network with rank based average pooling. *IEEE Access*, **5**, 16576–16583. <https://doi.org/10.1109/ACCESS.2017.2736558>.
- Wang, G., Li, W., Ourselin, S., & Vercauteren, T. (2017a). Automatic brain tumor segmentation using cascaded anisotropic convolutional neural networks. In *Brainlesion: Glioma, multiple sclerosis, stroke and traumatic brain injuries* (Vol. **10670**, pp. 178–190). [https://doi.org/10.1007/978-3-319-75238-9\\_16](https://doi.org/10.1007/978-3-319-75238-9_16).
- Wang, G., Li, W., Ourselin, S., & Vercauteren, T. (2019a). Automatic brain tumor segmentation based on cascaded convolutional neural networks with uncertainty estimation. *Frontiers in Computational Neuroscience*, **13**, 56. <https://doi.org/10.3389/FNCOM.2019.0056/BIBTEX>.
- Wang, M., Liu, X., Gao, Y., Ma, X., & Soomro, N. Q. (2017b). Superpixel segmentation: A benchmark. *Signal Processing: Image Communication*, **56**, 28–39. <https://doi.org/10.1016/j.image.2017.04.007>.
- Wang, S. H., Lv, Y. D., Sui, Y., Liu, S., Wang, S. J., & Zhang, Y. D. (2018a). Alcoholism detection by data augmentation and convolutional neural network with stochastic pooling. *Journal of Medical Systems*, **42**(1), 2. <https://doi.org/10.1007/s10916-017-0845-x>.
- Wang, S. H., Phillips, P., Sui, Y., Liu, B., Yang, M., & Cheng, H. (2018b). Classification of Alzheimer's disease based on eight-layer convolutional neural network with leaky Rectified Linear Unit and max pooling. *Journal of medical systems*, **42**(5), 42–85. <https://doi.org/10.1007/s10916-018-0932-7>.
- Wang, L., Wang, S., Chen, R., Qu, X., Chen, Y., Huang, S., & Liu, C. (2019b). Nested dilation networks for brain tumor segmentation based on magnetic resonance imaging. *Frontiers in Neuroscience*, **13**, 285. <https://doi.org/10.3389/FNINS.2019.00285>.
- Wang, S., Zhang, Y., Dong, Z., Du, S., Ji, G., Yan, J., Yang, J., Wang, Q., Feng, C., & Phillips, P. (2015). Feed-forward neural network optimized by hybridization of PSO and ABC for abnormal brain detection. *International Journal of Imaging Systems and Technology*, **25**(2), 153–164. <https://doi.org/10.1002/ima.22132>.
- Warfield, S. K., Kaus, M., Jolesz, F. A., & Kikinis, R. (2000). Adaptive, template moderated, spatially varying statistical classification. *Medical Image Analysis*, **4**(1), 43–55. [https://doi.org/10.1016/S1361-8415\(00\)00003-7](https://doi.org/10.1016/S1361-8415(00)00003-7).
- Wong, K.-P. (2005). Medical image segmentation: Methods and applications in functional imaging. In *Handbook of biomedical image analysis* (pp. 111–182). Springer.
- Wu, M.-N., Lin, C.-C., & Chang, C.-C. (2007). Brain tumor detection using adaptive k-means clustering segmentation. In *Proceedings of the 3rd International Conference on Intelligent Information Hiding and Multimedia Signal Processing (IIH-MSP 2007)* , (Vol. **2**, pp. 245–250). <https://doi.org/10.1109/IIHMSP.2007.4457697>.
- Xu, C., & Prince, J. L. (1997). Gradient vector flow: A new external force for snakes. In *Proceedings of the IEEE Computer Society Conference on Computer Vision and Pattern Recognition* (pp. 66–71). <https://doi.org/10.1109/cvpr.1997.609299>.
- Xu, C., & Prince, J. L. (1998). Generalized gradient vector flow external forces for active contours. *Signal Processing*, **71**(2), 131–139. [https://doi.org/10.1016/s0165-1684\(98\)00140-6](https://doi.org/10.1016/s0165-1684(98)00140-6).
- Xu, C., Pham, D., & Prince, J. (2000a). Image segmentation using deformable models. In *Handbook of medical imaging* (Vol. **2**, pp. 129–174). SPIE.
- Xu, C., Yezzi A., J., & Prince, J. L. (2000b). On the relationship between parametric and geometric active contours. In *Conference Record of the Thirty-Fourth Asilomar Conference on Signals, Systems*

- and Computers (Cat. No.00CH37154) (Vol. 1, pp. 483–489). <https://doi.org/10.1109/acssc.2000.911003>.
- Xu, L., Zeng, L., & Wang, Z. (2014). Saliency-based superpixels. *Signal, Image and Video Processing*, **8**(1), 181–190. <https://doi.org/10.1007/s11760-013-0520-8>.
- Xue, J. H., Pizurica, A., Philips, W., Kerre, E., Van De Walle, R., & Lemahieu, I. (2003). An integrated method of adaptive enhancement for unsupervised segmentation of MRI brain images. *Pattern Recognition Letters*, **24**(15), 2549–2560. [https://doi.org/10.1016/S0167-7865\(03\)00100-4](https://doi.org/10.1016/S0167-7865(03)00100-4).
- Yang, X., & Fei, B. (2011). A multiscale and multiblock fuzzy c-means classification method for brain MR images. *Medical Physics*, **38**(6), 2879–2891. <https://doi.org/10.1118/1.3584199>.
- Yang, G., Jones, T. L., Howe, F. A., & Barrick, T. R. (2016). Morphometric model for discrimination between glioblastoma multiforme and solitary metastasis using three-dimensional shape analysis. *Magnetic Resonance in Medicine*, **75**(6), 2505–2516. <https://doi.org/10.1002/mrm.25845>.
- Yang, T., Zhou, Y., Li, L., & Zhu, C. (2020). DCU-Net: Multi-scale U-Net for brain tumor segmentation. *Journal of X-Ray Science and Technology*, **28**(4), 709–726. <https://doi.org/10.3233/xst-200650>.
- Yousefi, S., Azmi, R., & Zahedi, M. (2012). Brain tissue segmentation in MR images based on a hybrid of MRF and social algorithms. *Medical Image Analysis*, **16**(4), 840–848. <https://doi.org/10.1016/j.media.2012.01.001>.
- Yu, F., & Koltun, V. (2015). Multi-scale context aggregation by dilated convolutions. *Proceedings of the 4th International Conference on Learning Representations, ICLR 2016*. <https://doi.org/10.48550/arxiv.1511.07122>.
- Zeiler, M. D., & Fergus, R. (2014). Visualizing and understanding convolutional networks. In *Proceedings of the European Conference on Computer Vision* (Vol. **8689**, pp. 818–833). [https://doi.org/10.1007/978-3-319-10590-1\\_53](https://doi.org/10.1007/978-3-319-10590-1_53).
- Zeiler, M. D., Krishnan, D., Taylor, G. W., & Fergus, R. (2010). Deconvolutional networks. In *2010 IEEE Computer Society Conference on Computer Vision and Pattern Recognition* (pp. 2528–2535). IEEE.
- Zhang, J., Jiang, Z., Dong, J., Hou, Y., & Liu, B. (2020). Attention gate ResU-Net for automatic MRI brain tumor segmentation. *IEEE Access*, **8**, 58533–58545. <https://doi.org/10.1109/ACCESS.2020.2983075>.
- Zhang, C., Shen, X., Cheng, H., & Qian, Q. (2019a). Brain tumor segmentation based on hybrid clustering and morphological operations. *International Journal of Biomedical Imaging*, **2019**, 7305832. <https://doi.org/10.1155/2019/7305832>.
- Zhang, Z., Wang, X., & Jung, C. (2019b). DCSR: Dilated convolutions for single image super-resolution. *IEEE Transactions on Image Processing*, **28**, 1625–1635. <https://doi.org/10.1109/TIP.2018.2877483>.
- Zhang, W., Yang, G., Huang, H., Yang, W., Xu, X., Liu, Y., & Lai, X. (2021). ME-Net: Multi-encoder net framework for brain tumor segmentation. *International Journal of Imaging Systems and Technology*, **31**(4), 1834–1848. <https://doi.org/10.1002/IMA.22571>.
- Zhao, L., & Jia, K. (2016). Multiscale CNNs for brain tumor segmentation and diagnosis. *Computational and Mathematical Methods in Medicine*, **2016**, 8356294. <https://doi.org/10.1155/2016/8356294>.
- Zhao, R., Niu, X., Wu, Y., Luk, W., & Liu, Q. (2017). Optimizing CNN-based object detection algorithms on embedded FPGA platforms. In *Applied reconfigurable computing* (Vol. **10216**, pp. 255–267). Springer. [https://doi.org/10.1007/978-3-319-56258-2\\_22](https://doi.org/10.1007/978-3-319-56258-2_22).
- Zhou, J., Chan, K., Chong, V., & Krishnan, S. (2005). Extraction of brain tumor from MR images using one-class support vector machine. In *2005 IEEE Engineering in Medicine and Biology 27th Annual Conference* (Vol. **7**, pp. 6411–6414). IEEE. <https://doi.org/10.1109/IEMB.2005.1615965>.
- Zhou, Z., He, Z., Shi, M., Du, J., & Chen, D. (2020). 3D dense connectivity network with atrous convolutional feature pyramid for brain tumor segmentation in magnetic resonance imaging of human heads. *Computers in Biology and Medicine*, **121**, 103766. <https://doi.org/10.1016/j.combiomed.2020.103766>.
- Zhou, X., Li, X., Hu, K., Zhang, Y., Chen, Z., & Gao, X. (2021). ERV-Net: An efficient 3D residual neural network for brain tumor segmentation. *Expert Systems with Applications*, **170**, 114566. <https://doi.org/10.1016/j.eswa.2021.114566>.
- Zikic, D., Ioannou, Y., Brown, M., & Criminisi, A. (2014). Segmentation of brain tumor tissues with convolutional neural networks. In *Proceedings of the MICCAI-BraTS* (pp. 36–39). <https://doi.org/10.1021/ol2032625>.